SENSORLESS SPEED CONTROL OF

PERMANENT MAGNET-ASSISTED SYNCHRONOUS RELUCTANCE MOTOR

(PMA-SYNRM)

A Thesis

by

ANIL KUMAR CHAKALI

Submitted to the Office of Graduate Studies of
Texas A&M University
in partial fulfillment of the requirements for the degree of

MASTER OF SCIENCE

December 2009

Major Subject: Electrical Engineering

SENSORLESS SPEED CONTROL OF

PERMANENT MAGNET-ASSISTED SYNCHRONOUS RELUCTANCE MOTOR

(PMA-SYNRM)

A Thesis

by

ANIL KUMAR CHAKALI

Submitted to the Office of Graduate Studies of
Texas A&M University
in partial fulfillment of the requirements for the degree of

MASTER OF SCIENCE

Approved by:

Chair of Committee,	Hamid A. Toliyat
Committee Members,	Mehrdad Ehsani
	Shankar Bhattacharyya
	Won-Jong Kim
Head of Department,	Costas Georghiades

December 2009

Major Subject: Electrical Engineering

ABSTRACT

Sensorless Speed Control of

Permanent Magnet-Assisted Synchronous Reluctance Motor

(PMa-SynRM). (December 2009)

Anil Kumar Chakali, B.E., Karnataka Regional Engineering College (now NITK)

Chair of Advisory Committee: Dr. Hamid Toliyat

An interesting alternative for today's high efficiency variable speed drives is the Permanent Magnet-Assisted Synchronous Reluctance Motor drive, which belongs to the family of brushless synchronous AC motor drives. Generally, the reluctance torque of this motor is significant compared to the Permanent Magnet electrical torque. The advantage of increased reluctance torque is the decreased need of expensive permanent magnet (PM) material, which makes this solution thus cheaper than the respective permanent magnet motor. Also due to its synchronous operation, sensorless rotational control is possible along with higher power factor and better efficiency compared to the induction motor (IM).

Therefore, this thesis first deals with the implementation of a vector control strategy for speed control of the PMa-synRM motor that can be applied to a washing machine application. The machine is supplied by a current controlled voltage source PWM inverter to control the instantaneous stator currents which are decided by the reference speed.

Secondly, the thesis focuses on the sensorless speed operation of the PMa-SynRM to take advantage of the lower costs as well as increased system reliability which otherwise is not possible using the delicate speed or position sensors. The concept involves estimation of the rotor speed and/or position. There are several speed estimation techniques proposed by researchers and among them the observer based technique is proven and commonly used in the industry. The only requirements of the observer system are a very fast signal processor, specialized and optimized to perform complex mathematical calculations.

The feasibility and effectiveness of the control techniques are verified using the experimental results, implemented using the Texas Instruments TMS320F2812 eZDSP controller board and the overall motor drive system in the laboratory.

Dedicated to my parents and my sister

ACKNOWLEDGEMENTS

I wish to express my deep gratitude to my advisor, Prof. Hamid A. Toliyat, for his constant support, encouragement and guidance. I wish to thank my committee members: Prof. Mehrad Ehsani, Prof. Shankar Bhattacharyya, Prof. Wong-Jong Kim and Prof. Karen L. Butler-Purry for their time and support.

Thanks also go to my friends and colleagues at Advanced Electric Machine and Power Electronics Laboratory for their help, particularly Robert Vartanian, Jeihoon Baek, Behrooz Nikbakhtan, Nicholas Frank, Suengdeog Choi, Mashid Amirabadi, Mehran Mirjafari, Vivek Sundaram, Anand Balakrishnan, Yateendra Deshpande, Dr. Salman Talebi and Dr. Baris Ozturk.

Finally, I would like to express my sincere appreciation to my mother, father and sister for their patience, support and encouragement.

TABLE OF CONTENTS

CHAPTER Page

LIST OF FIGURES

FIGURE Page

FIGURE Page

FIGURE Page

LIST OF TABLES

CHAPTER I

INTRODUCTION

1.1 Background

During the recent years there has been a considerable increase of interest in using brushless synchronous AC machines in variable speed applications where previously asynchronous machines have been used [1-6]. Among the AC drives, the permanent magnet synchronous machine (PMSM) drives have been increasingly applied in a wide variety of industrial applications. The reason comes from the advantages of PMSM which are high power density and efficiency, high torque to inertia ratio and high reliability. However, recently the high cost of magnet materials (e.g., samarium cobalt and neodymium-boron iron) and the possibility of the Permanent Magnets demagnetization at higher speeds is restricting its applications to some extent [7].

So an interesting alternative for today's high efficiency variable speed drives is the Permanent Magnet-Assisted Synchronous Reluctance Motor (PMa-SynRM) drive, which belongs to the family of brushless synchronous AC motor drives [7]. The PMa-SynRM is a combination of permanent magnet synchronous motor and synchronous reluctance motor. Generally the share of the reluctance torque is significant compared to the PM electrical torque. So this motor can mainly be treated as a synchronous reluctance motor. A conventional three phase inverter can be used to drive this motor.

This thesis follows the style and format of *IEEE Transactions on Industry Applications*.

With the rapid development of microprocessors (μC) and digital signal processors (DSP), vector control is becoming a common technique for synchronous motor drive systems, especially in the low-cost applications such as home appliance and machine tools. The vector control (or called field-oriented control) of AC machines was introduced in the late 1960s by Blaschke, Hasse, and Leonhard in Germany. Following their pioneering work, this technique has allowed for the quick torque response of AC machines similar to that of DC machines. So this technique has achieved a high degree of maturity and become popular in a broad variety of applications. It is also widely applied in many areas where servo-like high performance plays a secondary role to reliability and energy savings.

Knowledge of the rotor position is very important in the field-oriented control. Usually the rotor position is measured by using electromagnetic resolvers or digitally by using incremental or absolute encoders. Optical encoders are one of the most widely used position sensors. Electromagnetic resolvers are popular too because of their rugged construction and higher operating temperature. However, the presence of such sensors not only increases the cost and hardware complexity of the overall drive system but also reduces its control robustness and reliability. Furthermore, it might be difficult to install and maintain a position sensor due to the limited assembly space and rigid working environment with severe vibration and/or high temperature. It also increases the system inertia, which is undesirable in high-performance drives. In very small motors, it is impossible to use electromechanical sensors. Therefore, various position-sensorless

control schemes have been developed for the estimation of rotor position and speed, especially during the last decade [8-12].

The advantages of PMa-SynRM, namely the power density, efficiency, flux weakening and high temperature operation capability compared to the same size asynchronous motors, makes them highly attractive for "direct drive" applications, such as hybrid electrical vehicles (HEV) and washing machines. In washing machines, the rotating working unit of a direct drive system, such as the basket or drum, can be coupled directly to the motor shaft without the need for transmission assembly, such as clutches, belts, pulleys and/or gearboxes. The power is directly delivered to the working unit by the motor. This concept of direct drive has the following advantages: high dynamic response, increased efficiency, low acoustic noise, and long lifetime due to the elimination of the transmission components. Such direct drive applications normally require large shaft torque at standstill (i.e., zero speed) and low speeds as well as constant output power over wide speed range. In order to meet these requirements, the PMa-SynRM machines are designed to operate not only in the constant torque region where the motor speed is below the rated or base speed but also in the constant power region where the motor speed is above the rated speed. In this way, the cost and size of the overall drive system can be significantly reduced. The constant torque of the PMa-SynRM can be achieved by the conventional vector control. For speeds above the base speed, the flux weakening control method needs to be applied to weaken the air-gap flux [13-16].

This thesis will discuss the sensorless vector control technique for PMa-SynRM in the constant torque region and beyond that.

1.2 Objectives of the Study

This thesis studies the feasibility of sensorless vector control of PMa-SynRM that can be applied to a direct drive system such as washing machine. An experimental PMa-SynRM drive system was designed and built at the Texas A&M University (TAMU).

The main objectives of this research work include:

1. Develop a robust, efficient speed control scheme using a low cost DSP based controller.
2. Develop an observer for estimating the rotor position and hence the speed for sensorless operation.

1.3 Thesis Outline

This thesis is outlined as follows:

Chapter I introduces the background of the thesis and the main goals.

Chapter II covers the background information on synchronous reluctance motor. A brief history of this motor is presented. Then it reviews the recent developments in modern synchronous drives and position-sensorless control techniques.

Chapter III addresses the mathematical modeling and control strategies of PMa-SynRM machines. The principle of vector control for constant torque and constant power regions is investigated.

Chapter IV presents a sliding mode technique for position-sensorless control of PMa-SynRM.

Chapter V presents the system implementation and laboratory results on a 380W PMa-SynRM machine.

Chapter VI gives the major conclusions.

CHAPTER II

LITERATURE

2.1 Evolution of Synchronous Reluctance Motor

The principle of using the difference of reluctance to produce the torque has been known for over 160 years. Before the discovery of the rotating magnetic field by Tesla in 1887, the first reluctance motor was similar to the doubly salient synchronous reluctance motor, nowadays known as the switched reluctance motor. The first rotating magnetic-field synchronous motor was, however, introduced by Kostko not earlier than in 1923 (Kostko 1923).

There are different designations for singly salient synchronous reluctance motors in the literature. The most popular names for this motor are: Reluctance motor (RM), Synchronous Reluctance Motor (SRM, Synchrel, SynRM) and Reluctance Synchronous Motor (RSM). Figure 2-1 shows a cross-sectional view of a single saliency RM consisting of a non-salient stator and a two-pole salient rotor, both made of high permeability magnetic material. This figure shows a three-phase stator winding although any number of phases is possible. Figure 2-2 shows the cross-sectional view of a three phase double saliency RM.

In principle, the SynRM is similar to the traditional salient pole synchronous motor but does not have an excitation winding in its rotor. In this case only the rotor is constructed with salient poles. The stator inner surface is cylindrical and typically retains

many of the benefits of variable reluctance motors and at the same time eliminates its several disadvantages. Before the development of today's AC motor drives, in a variable speed drive, motor was supplied from a fixed frequency power source. In this case, it was necessary that the SynRM includes a squirrel cage on the rotor to provide the starting torque for line-start. Otherwise, the rotor could not accelerate and synchronize with the supplying network. The squirrel cage was also needed as a damper winding in order to maintain synchronism under sudden load torques. The presence of a cage for line starting in the rotor structure was interfering with the requirements of the optimum rotor design.

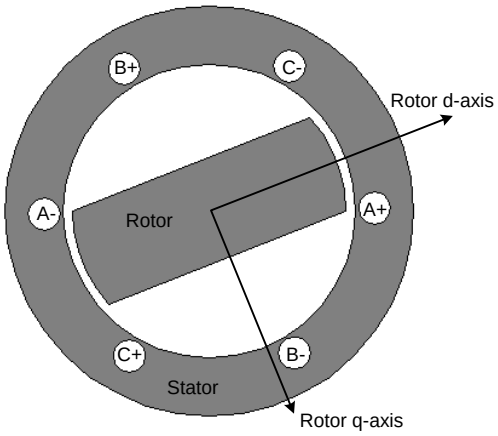

Figure 2-1 Basic three phase, two pole reluctance variable motor, single saliency SynRM

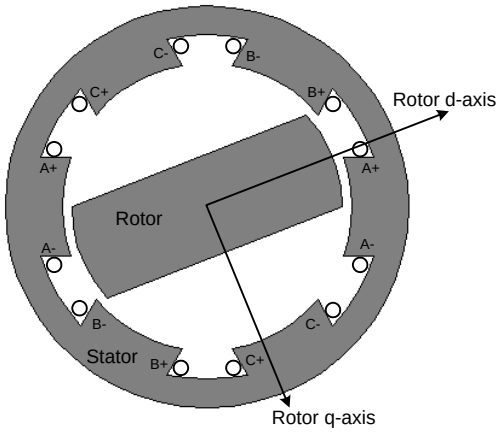

Figure 2-2 Basic three phase, two pole reluctance variable motor, double saliency switch reluctance motor

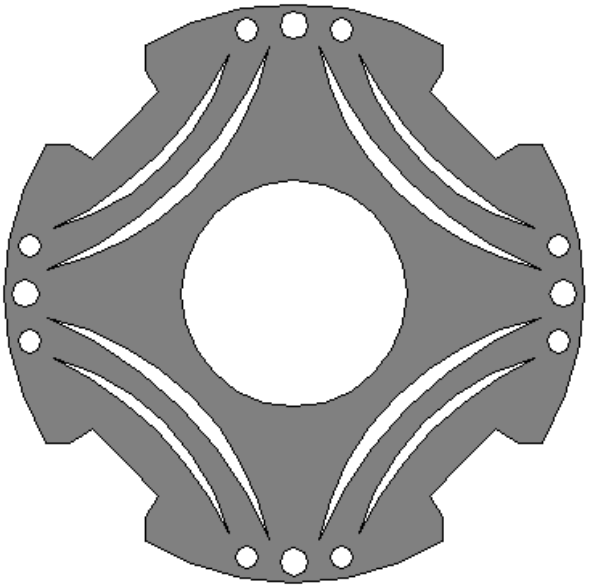

Figure 2-3 Flux barrier type rotor of reluctance motor of the sixties

Figure 2-3 shows a sketch of a typical machine of that era which utilized the flux barriers to form a difference in saliency between the polar axis (d-axis) and interpolar axis (q-axis). In most cases, inverters of these motors were not able to operate below 10Hz. Therefore, the motors were typically line started (asynchronously started) with the

inverter frequency set at about 10Hz. After being synchronized with the supplied frequency, motor could continue its operation above 10Hz and proceed with the inverter frequency. Over the desired speed range, the inverter was controlled to supply a constant volt/hertz which approximately results in a constant air gap flux. Since the inverter frequency was not generally controlled such that it damps the load oscillations, stability problems was occurred related to the "swing" of a synchronous machine operating from a fixed 60Hz supply. In fact, it has been shown that complete instability resulting in continuous speed oscillations around the nominal speed could occur without corrective action. In addition, a “pull in” phenomenon occurred when the motor was started up with a load. In this case, since starting torque is an inductive torque and is generated by an incomplete cage, as in Figure 2-3, synchronism with the inverter was not always achieved during the asynchronous start. Therefore, it resulted in continuous operation as an induction motor rather than a synchronous motor. In this case, generated torque had a large torque pulsation. Consequently, this large torque pulsation resulted in substantial speed oscillation. Finally, sudden change in loading of the machine resulted in loss of synchronism with the power source frequency.

These problems were of course very detrimental to the application which demanded precise speed control. Moreover, ratio of the d axis inductance over q axis inductance (saliency ratio) of such machines could not exceed much more than 2:1. Because of the low saliency ratio, frame size of this motor was larger than an equivalent induction motor. Nonetheless, such machines were used for many years and continued to

be manufactured. However, they have been largely replaced by permanent magnet synchronous motors in the fiber spinning application.

Developments in machine design and power electronics allowed the machine designers to remove the starting cage from the rotor and achieve a better performance by using field oriented (vector) control. In vector controlled drives, two crucial parameters are the difference of d and q axes inductances $(L_d - L_q)$, as in the line-start case, and the ratio of these two inductances (L_d / L_q) [17, 18, 19]. A variety of vector controlled strategies have been introduced in literature and it turns out that the best performance for all of them is obtained if these two parameters are made as large as possible. In order to fulfill this requirement, the rotor should be designed for maximum L_d and minimum L_q.

2.2 Permanent Magnet-Assisted Synchronous Reluctance Motor

When PMs are inserted into the rotor flux barriers of a synchronous reluctance motor, it becomes a permanent magnet-assisted synchronous reluctance motor (PMa-SynRM). PMs can be mounted in the rotor core of the axially or transversally laminated structure. Figure 2-4 shows a transversally laminated PMa-SynRM. The polarity of magnets is chosen such that it counteracts the q-axis flux of the SynRM at rated load. Regardless of the different choice of d, q axes, in principle, the PMa-SynRM seems nothing more than a particular case of interior permanent magnet motor (IPM). However, a substantial difference is the high anisotropy rotor structure of PMa-SynRM and as a result, low value of the PM flux. The amount of PM flux is quite lower than the

amount of rated flux. In contrast, in the usual IPM the most flux comes from the magnets and the flux produced by stator currents is considered as an unwanted reaction flux. In practice, because of the above mentioned difference between PMa-SynRM and IPM machines, they have different suitability to the large flux-weakening ranges.

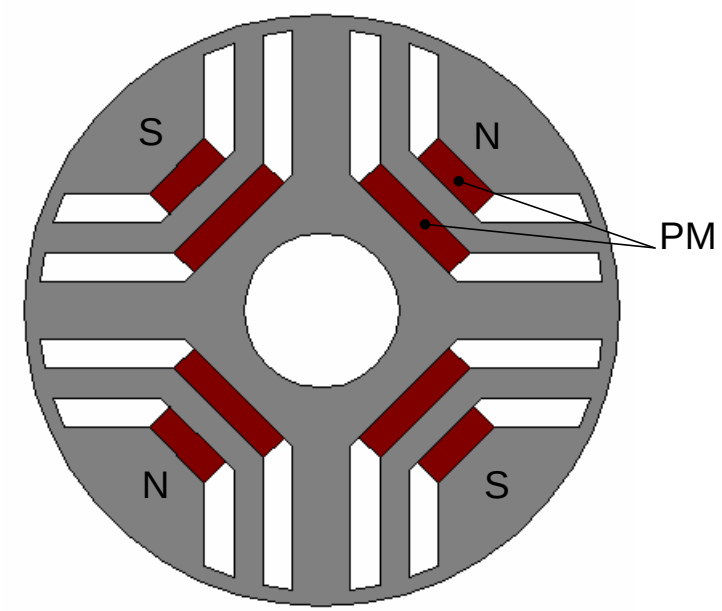

Figure 2-4 Transversally-laminated PM assisted rotor

2.3 Modern Synchronous Drives

With the development of new technology, particularly in the areas of digital electronics and power semiconductor devices, performance of synchronous drives has drastically improved. Current controlled PWM inverters along with the field oriented (vector) control [20] have significantly contributed to the revival of interest in the SynRM over the last few years. Enhancement of drive performance and stable synchronous operation down to very low speeds including standstill has been possible by

use of vector control [21]. Achieving this operation was difficult by use of conventional V/F control [22].

Inserting magnets in the rotor flux barriers is another way to improve the performance of the motor [23] which changes the motor from SynRM to PMa-SynRM. Beside better design of the motor, the enhancement of the overall drive could be possible by using more advance control algorithms. Due to advent of high speed microprocessors implementation of the advanced control procedures have been possible. Most of the modern control algorithms are model based and are parameter dependent. The main limitation of most of the works on the optimal control of SynRM is use of an ideal model in order to perform theoretical analysis and practical implementation [24]. However, in a real machine the effects of saturation and iron losses result in deviation of the current angle from the optimal operating point. So knowledge of the motor parameters and also use of a more realistic model is crucial in order to implement an optimal control.

2.4 Review of Sensorless Techniques

In the past few years, great efforts have been made to introduce speed and/or shaft position sensorless torque controlled drives. These drives are usually referred to as “sensorless” drives, although the terminology “sensorless” refers to only the speed and shaft sensors; there are still other sensors in the drive system (e.g., current sensors), since closed loop operation cannot be performed without them.

Wu and Slemon [25] used the back-EMF estimated from the measurement of terminal voltages and stator currents. Integration of the machine terminal voltages yields

the rotor flux quantities from which the rotor angle information was obtained. This method suffered from limitations at low speed because the back-EMF generated is proportional to the speed, and at low speeds the back-EMF is very low and difficult to extract it from the switching noise of the inverter driving the motor.

Using the measured current and voltage, which are then transformed using rotor and stator d-q frames, the stator frame voltage equations can be manipulated to yield rotor angle [26, 27, 28]. However these methods usually suffer from the poor precision and offset problems of the integral algorithm and the low accuracy of differential operation as well as the low speed operation which is similar to the above back-EMF method.

Observer principles have been popular in recent years and are preferred for medium to high-speed operations. Extended Kalman filter (EKF) is used as a position estimator in [29, 30]. The limitations of the EKF, such as guaranteeing the convergence of the estimated positions and the computational complexity, have hindered in its widespread use. Other observer systems include non-linear, full-order, disturbance, reduced order, sliding mode and etc [31, 32, 33, 34, 35, 36]. Compared with the other observers, the sliding mode observer which is similar to the sliding controller is more robust to disturbances and less sensitive to parameter variations, hence is an important candidate for the state estimator in rotor position and speed. The only limitation with sliding mode observer is the lack of initial information of the state which can result in deteriorating performance at zero and around low speeds.

In the case of motors with rotor saliencies, the rotor position can be estimated using the inherent rotor saliency [37, 38, 39]. Since the rate of current change depends on the inductance of the winding, and this inductance is a function of rotor position and winding current, then rotor position can be deduced from winding current and its rate of change. This scheme has the important advantage that it is useful even at zero speed where there is no motional EMF. An "INFORM" method was proposed by Schroedl, which was based on real-time inductance measurements using saliency and saturation effects. During a short time interval, the "complex INFORM reactance" was calculated for estimating flux angle [40]. On the other hand, Corley and Lorenz investigated a high frequency signal injection method in such a way that carrier-frequency voltages were applied to the stator windings of PMSM, producing high-frequency currents of which the magnitude varies with rotor position. The sensed currents were then processed with a heterodyning technique that produced a signal approximately proportional to the difference between the actual and the estimated rotor position [41]. However, all these methods require high-precision and high-bandwidth (fast) measurement and fast signal processing capability, which inevitably increase the complexity and cost of control system. The injected high-frequency voltages may also cause more torque ripple, shaft vibration and audible noises. Furthermore, due to the constraints of the maximum PWM switching frequency and the geometry of rotor, such methods usually work to some specific motors in the limited operating speed range, i.e., only at standstill and low speeds.

In addition, fuzzy-logic, neural network and artificial intelligence-based estimators have been presented for the sensorless control of PMSM [42, 43, 44]. These methods use artificial neural network (ANN), diagonally recurrent neural network or fuzzy-neural network combined with adaptive technique. They are completely different from traditional model-based estimation methods as discussed above. Moreover, artificially intelligent estimators are relatively complicated and require large computation time, which must be implemented in a high-performance and expensive microprocessor or DSP that is not suitable for cost-effective drive systems.

CHAPTER III

MODELING, OPERATION AND CONTROL OF PERMANENT MAGNET-ASSISTED SYNCHRONOUS RELUCTANCE MOTOR

3.1 Introduction

This chapter systemically reviews mathematical model of the Permanent Magnet Assisted-Synchronous Reluctance motor and then proceeds to design the control algorithms. Transformations of variables are used to deal with the time-varying machine inductances, referring to the coefficients of differential equations (e.g., voltage equations) that describe the performance and behavior of the PMa-SynRM motor. All the basic principles of PMa-SynRM machine are discussed for vector control implementation.

3.2 Mathematical Model of PMa-SynRM in the Stationary Reference Frame

For the purpose of understanding and designing control schemes for PMa-SynRM drive, it is necessary to know the dynamic model of PMa-SynRM subjected to control. The mathematical model of the PMa-SynRM is similar to that of the wound rotor synchronous motor except that the excitation (field) winding does not exist. Moreover, in machines typically employing a modern axially or transversally laminated rotor structure, a rotor cage is normally absent because the machine can start from zero speed by proper inverter control.

Mathematical models valid for instantaneous variation of voltage and current adequately describing the performance of synchronous motor in both steady state and transient are commonly obtained by the utilization of space-phasor theory. Figure 3-1 shows the cross-section view of a simplified symmetrical three-phase, two-pole Synchronous Motor with wye-connected concentrated identical stator windings. These, however, represent distributed windings which at every instant produce sinusoidal MMF waves centered on the magnetic axes of the respective phases. The phase windings are displaced by 120 electrical degrees from each other. In Figure 3.1, θ_r is the rotor position angle, which is between the magnetic axes of stator winding sA and rotor d-axis. The angular velocity of rotor is calculated by $\omega_r = d\theta_r / dt$, and its positive direction is also shown.

It is assumed that the permeability of iron parts of the synchronous motor under consideration is infinite and the flux density distribution is radial in the air-gap. The effects of iron losses, saturation and end-effects are neglected. The analysis given is valid for linear magnetic circuits.

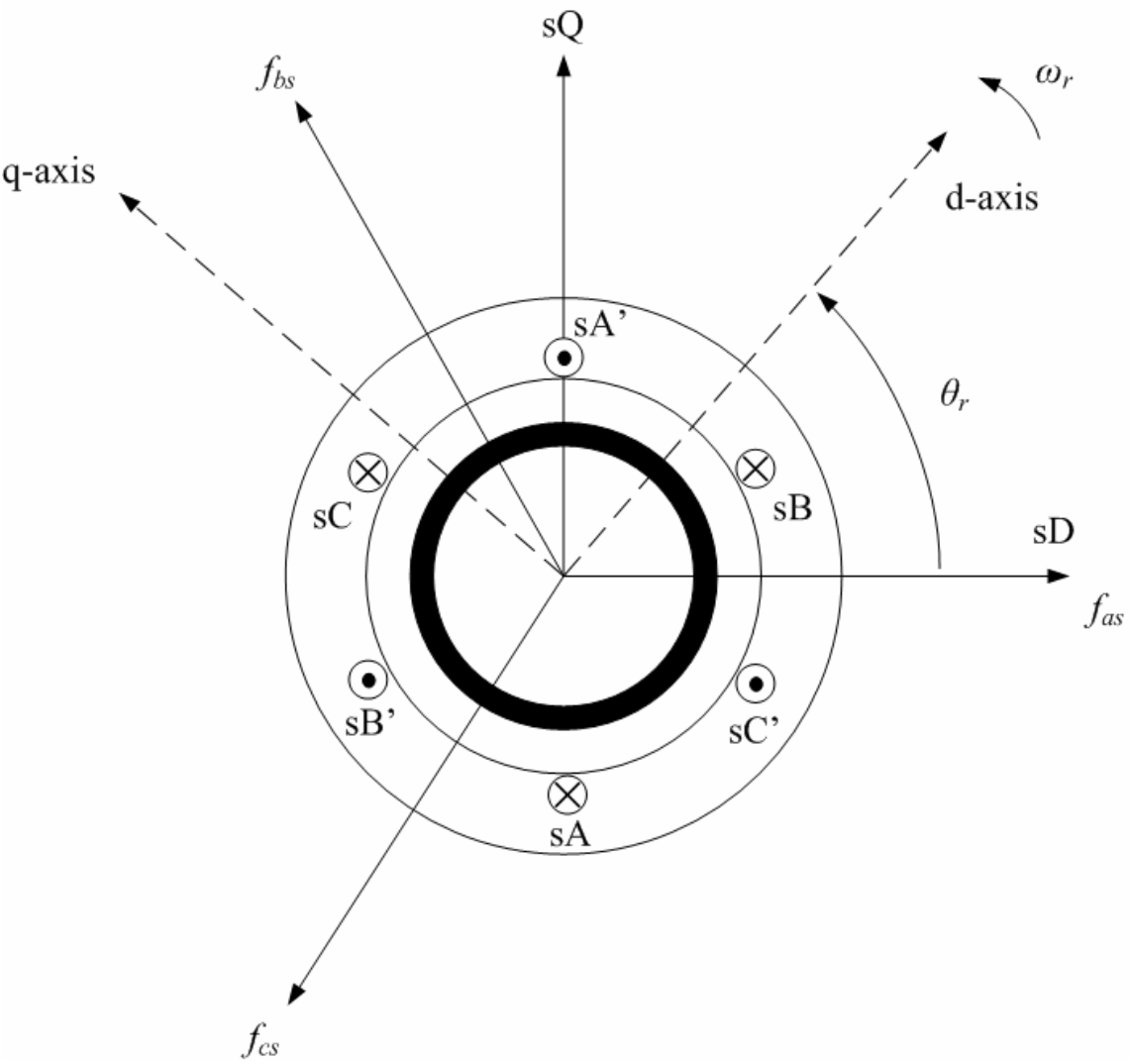

Figure 3-1 Cross-section view of a simplified symmetrical three-*phase, two-pole SM*

3.2.1 General Model of Synchronous Motor with Saliency

Using polarity convention for phase currents and voltages of a SM, its voltage equations can be expressed in terms of instantaneous currents and flux linkages by

$$\vec{v}_{abcs} = r_{abcs} \cdot \vec{i}_{abcs} + p \cdot \vec{\lambda}_{abcs} \qquad (3.1)$$

where

$$\vec{v}_{abcs} = [v_{as} \quad v_{bs} \quad v_{cs}]^T$$

$$\vec{i}_{abcs} = [i_{as} \quad i_{bs} \quad i_{cs}]^T$$

$$\vec{\lambda}_{abcs} = [\lambda_{as} \quad \lambda_{bs} \quad \lambda_{cs}]^T$$

$$r_{abcs} = diag[R_s \quad R_s \quad R_s]$$

In the above, the 's' subscript denotes variables and parameters associated with the stator circuits, and 'r'subscript denotes those with the rotor circuits. The operator 'p' represents the differential operator d/dt. For a magnetically linear system, the flux linkages can be calculated as follows:

$$\vec{\lambda}_{abcs} = L_{abcs} \cdot \vec{i}_{abcs} + \vec{\lambda}_{abcm} \tag{3.2}$$

where

$$L_{abcs} = \begin{bmatrix} L_{aa} & L_{ab} & L_{ac} \\ L_{ba} & L_{bb} & L_{bc} \\ L_{ca} & L_{cb} & L_{cc} \end{bmatrix}$$

$$\vec{\lambda}_{abcm} = \lambda_m \begin{bmatrix} \sin\theta_r \\ \sin(\theta_r - 2\pi/3) \\ \sin(\theta_r + 2\pi/3) \end{bmatrix}$$

where the winding inductances are,

$$L_{aa} = L_{ls} + L_{0s} + L_{2s}\cos 2\theta_r$$

$$L_{bb} = L_{ls} + L_{0s} + L_{2s}\cos 2(\theta_r - 2\pi/3)$$

$$L_{cc} = L_{ls} + L_{0s} + L_{2s}\cos 2(\theta_r + 2\pi/3)$$

$$L_{ab} = L_{ba} = -\frac{1}{2}L_{0s} + L_{2s}\cos 2(\theta_r - \pi/3)$$

$$L_{ac} = L_{ca} = -\frac{1}{2}L_{0s} + L_{2s}\cos 2(\theta_r + \pi/3)$$

$$L_{bc} = L_{cb} = -\frac{1}{2}L_{0s} + L_{2s}\cos 2(\theta_r + \pi)$$

In the above, L_{ls} is the leakage inductance and L_{0s} and L_{2s} are the magnetizing inductance components of the stator windings; λ_m is the flux linkage established by the rotor magnets. It should be noted that the magnetizing inductance components are functions of the rotor position; and the coefficient L_{2s} is negative while L_{0s} is positive in the case of interior PM motors due to their unique rotor structure. Therefore, the quadrature-axis magnetizing inductance L_{mq} is larger than the direct-axis magnetizing inductance L_{md} of interior PM motor, which is opposite to general salient-pole synchronous machines.

The flux linkage equation can be extended to the form of

$$\begin{bmatrix} \lambda_{as} \\ \lambda_{bs} \\ \lambda_{cs} \end{bmatrix} = \begin{bmatrix} L_{aa} & L_{ab} & L_{ac} \\ L_{ba} & L_{bb} & L_{bc} \\ L_{ca} & L_{cb} & L_{cc} \end{bmatrix} \begin{bmatrix} i_{as} \\ i_{bs} \\ i_{cs} \end{bmatrix} + \lambda_m \begin{bmatrix} \sin\theta_r \\ \sin(\theta_r - 2\pi/3) \\ \sin(\theta_r + 2\pi/3) \end{bmatrix} \qquad (3.3)$$

From the two-axis theory, an equivalent quadrature-phase machine is used to represent the three-phase machine, in which the direct- and quadrature-axis currents, fictitious components, are flowing in virtual windings and are related to the actual three-phase stator currents as follows:

$$\vec{i}_{\alpha\beta 0s} = T_{abc\to\alpha\beta 0} \cdot \vec{i}_{abcs} \qquad (3.4)$$

where

$$T_{abc\to\alpha\beta 0}=\frac{2}{3}\begin{bmatrix}1 & -1/2 & -1/2\\ 0 & \sqrt{3}/2 & -\sqrt{3}/2\\ 1/2 & 1/2 & 1/2\end{bmatrix}$$

The above transformation of variables is also known as Clark Transformation. Then the new stationary reference frame referring to the quadrature-phase machine is called (α-β) frame. Whereas, the previous stationary frame is called (a-b-c) frame.

Similarly, voltage and flux linkage variables can be transformed from (a-b-c) frame to (α-β) frame and consequently the voltage equations expressed in the (α-β) frame as:

$$\vec{v}_{\alpha\beta 0s}=r_{\alpha\beta 0s}\cdot\vec{i}_{\alpha\beta 0s}+p\cdot\vec{\lambda}_{\alpha\beta 0s} \qquad (3.5)$$

where

$$\vec{v}_{\alpha\beta 0s}=[v_{\alpha s}\quad v_{\beta s}\quad v_{0s}]^T$$

$$\vec{i}_{\alpha\beta 0s}=[i_{\alpha s}\quad i_{\beta s}\quad i_{0s}]^T$$

$$\vec{\lambda}_{\alpha\beta 0s}=[\lambda_{\alpha s}\quad \lambda_{\beta s}\quad \lambda_{0s}]^T$$

The flux linkages change to

$$\vec{\lambda}_{\alpha\beta 0s}=L_{\alpha\beta 0s}\cdot\vec{i}_{\alpha\beta 0s}+\vec{\lambda}_{\alpha\beta 0m} \qquad (3.6)$$

where

$$L_{\alpha\beta 0s}=\begin{bmatrix}L_{ls}+\frac{3}{2}(L_{0s}+L_{2s}\cos 2\theta_r) & \frac{3}{2}L_{2s}\sin 2\theta_r & 0\\ \frac{3}{2}L_{2s}\sin 2\theta_r & L_{ls}+\frac{3}{2}(L_{0s}-L_{2s}\cos 2\theta_r) & 0\\ 0 & 0 & L_{ls}\end{bmatrix}$$

$$\vec{\lambda}_{\alpha\beta 0m} = \lambda_m \begin{bmatrix} \sin\theta_r \\ -\cos\theta_r \\ 0 \end{bmatrix}$$

Provided that the stator windings are in wye-connected arrangement with floating neutral point and supplied with three-phase currents, which vary arbitrarily in time, the sum of the three phase currents are always equal to zero regardless of three-phase balanced condition. As a result, the 0-axis component of current variable in the (α-β) frame, i.e., i_{0s}, is zero and so are the 0-axis components of voltage and flux linkage variables. Therefore, the (3.5) to (3.6) can be reduced to

$$\vec{v}_{\alpha\beta s} = r_{\alpha\beta s} \cdot \vec{i}_{\alpha\beta s} + p \cdot \vec{\lambda}_{\alpha\beta s} \qquad (3.7)$$

where

$$\vec{v}_{\alpha\beta s} = [v_{\alpha s} \quad v_{\beta s}]^T$$

$$\vec{i}_{\alpha\beta s} = [i_{\alpha s} \quad i_{\beta s}]^T$$

$$\vec{\lambda}_{\alpha\beta s} = [\lambda_{\alpha s} \quad \lambda_{\beta s}]^T$$

The flux linkage becomes,

$$\vec{\lambda}_{\alpha\beta s} = L_{\alpha\beta s} \cdot \vec{i}_{\alpha\beta s} + \vec{\lambda}_{\alpha\beta m} \qquad (3.8)$$

where

$$L_{\alpha\beta s} = \begin{bmatrix} L_{ls} + \frac{3}{2}(L_{0s} + L_{2s}\cos 2\theta_r) & \frac{3}{2}L_{2s}\sin 2\theta_r \\ \frac{3}{2}L_{2s}\sin 2\theta_r & L_{ls} + \frac{3}{2}(L_{0s} - L_{2s}\cos 2\theta_r) \end{bmatrix}$$

$$\vec{\lambda}_{\alpha\beta m} = \lambda_m \begin{bmatrix} \sin\theta_r \\ -\cos\theta_r \end{bmatrix}$$

3.3 Mathematical Model of PMa-SynRM in the Rotating Reference Frame

In late 1920s, R. H. Park introduced a new approach to implement change of variables, which replaces variables (voltages, currents, and flux linkages) associated with stator windings of a synchronous machine with variables associated with fictitious windings rotating with the rotor. Park's transformation eliminates all time-varying inductances from the voltage equations of the synchronous machine which occur due to electric circuits both in relative motion and with varying magnetic reluctance [45]. The transformation, namely Park Transformation, and its inversion can be mathematically expressed in the following:

$$f_{dq0s} = T_{abc\to dqo} \cdot f_{abcs} \tag{3.9}$$

where

$$T_{abc\to dq0} = T_{\alpha\beta0\to dq0} T_{abc\to\alpha\beta0} = \frac{2}{3}\begin{bmatrix} \cos\theta & \cos(\theta-2\pi/3) & \cos(\theta-4\pi/3) \\ -\sin\theta & -\sin(\theta-2\pi/3) & -\sin(\theta-4\pi/3) \\ 1/2 & 1/2 & 1/2 \end{bmatrix}$$

$$T_{\alpha\beta0\to dq0} = \begin{bmatrix} \cos\theta & \sin\theta & 0 \\ -\sin\theta & \cos\theta & 0 \\ 0 & 0 & 1 \end{bmatrix}$$

The inverse transformation, namely inverse park transformation is

$$f_{abcs} = T_{dqo\to abc} \cdot f_{dq0s} \tag{3.10}$$

where

$$T_{dq0\to abc} = (T_{abc\to dq0})^{-1} = \begin{bmatrix} \cos\theta & -\sin\theta & 1 \\ \cos(\theta - 2\pi/3) & -\sin(\theta - 2\pi/3) & 1 \\ \cos(\theta - 4\pi/3) & -\sin(\theta - 4\pi/3) & 1 \end{bmatrix}$$

In the above equations, $\boldsymbol{f}$ can represent either voltage, current or flux linkage vector variables. The angular displacement θ should be continuous; however, the angular velocity is unspecified and can be selected arbitrarily to expedite the solution of system equations or to satisfy system constraints. The frame of reference may rotate at any constant or varying angular velocity or it may remain stationary as in the Clark Transformation.

For a three-phase balanced system, the park transformation can be reduced to

$$T_{abc\to dq} = \frac{2}{3}\begin{bmatrix} \cos\theta & \cos(\theta - 2\pi/3) & \cos(\theta - 4\pi/3) \\ -\sin\theta & -\sin(\theta - 2\pi/3) & -\sin(\theta - 4\pi/3) \end{bmatrix}$$

3.3.1 General Model of Synchronous Motor with Saliency

In terms of the variables in the rotating reference frame aligned with rotor flux, i.e., rotor reference frame, the voltage equation (3.5) becomes

$$\vec{v}_{dq0s} = r_s \cdot \vec{i}_{dq0s} + T_{abc\to dq0} \cdot p[(T_{abc\to dq0})^{-1}]\vec{\lambda}_{dq0s} + p\vec{\lambda}_{dq0s} \qquad (3.11)$$

where

$$\vec{v}_{dq0s} = [v_{ds} \quad v_{qs} \quad v_{0s}]^T$$

$$\vec{i}_{dq0s} = [i_{ds} \quad i_{qs} \quad i_{0s}]^T$$

$$\vec{\lambda}_{dq0s} = [\lambda_{ds} \quad \lambda_{qs} \quad \lambda_{0s}]^T$$

The stator flux linkage viewed in the rotor reference frame is given by,

$$\vec{\lambda}_{dq0s} = L_{dq0s} \cdot \vec{i}_{dq0s} + \vec{\lambda}_{dq0m} \tag{3.12}$$

where

$$\vec{\lambda}_{dq0m} = [0 \quad \lambda_m \quad 0]^T$$

$$L_{dq0s} = \begin{bmatrix} L_d & 0 & 0 \\ 0 & L_q & 0 \\ 0 & 0 & L_0 \end{bmatrix}$$

$$L_d = L_{ls} + L_{md} = L_{ls} + \frac{3}{2}(L_{0s} + L_{2s})$$

$$L_q = L_{ls} + L_{mq} = L_{ls} + \frac{3}{2}(L_{0s} - L_{2s})$$

$$L_0 = L_{ls}$$

L_{0s} and L_{2s} can be expressed as

$$L_{0s} = \frac{2}{3}\left(\frac{L_{md} + L_{mq}}{2}\right) = \frac{1}{3}\left(L_{md} + L_{mq}\right)$$

$$L_{2s} = \frac{2}{3}\left(\frac{L_{md} - L_{mq}}{2}\right) = \frac{1}{3}\left(L_{md} - L_{mq}\right)$$

L_d is named as the direct-axis stator inductance and L_q is the quadrature-axis stator inductance.

It is easy to show,

$$p\left[(T_{abc\to dq0})^{-1}\right] = \omega_r \begin{bmatrix} -\sin\theta & -\cos\theta & 0 \\ -\sin(\theta - 2\pi/3) & -\cos(\theta - 2\pi/3) & 0 \\ -\sin(\theta - 4\pi/3) & -\cos(\theta - 4\pi/3) & 0 \end{bmatrix} \tag{3.13}$$

Thus,

$$T_{abc\to dq0}\, p\left[(T_{abc\to dq0})^{-1}\right] = \omega_r \begin{bmatrix} 0 & -1 & 0 \\ 1 & 0 & 0 \\ 0 & 0 & 0 \end{bmatrix} \tag{3.14}$$

Equation (3.11) in terms of d and q components is

$$v_{ds} = R_s i_{ds} + L_d \frac{di_{ds}}{dt} - \omega_r L_q i_{qs} + \omega_r \lambda_m \tag{3.15}$$

$$v_{qs} = R_s i_{qs} + L_q \frac{di_{qs}}{dt} + \omega_r L_d i_{ds} \tag{3.16}$$

$$v_{0s} = R_s i_{0s} + L_0 \frac{di_{0s}}{dt} \tag{3.17}$$

Under balanced steady-state conditions, the electrical angular velocity of rotor ω_r is considered constant and equal to that of the synchronously rotating reference frame. In this mode of operation, with the time rate of change of all flux linkages neglected, the steady state versions of (3.15), (3.16) and (3.17) become

$$V_{ds} = R_s I_{ds} - \omega_r L_q I_{qs} + \omega_r \lambda_m \tag{3.18}$$

$$V_{qs} = R_s I_{qs} + \omega_r L_d I_{ds} \tag{3.19}$$

$$V_{0s} = R_s I_{0s} = 0 \tag{3.20}$$

The upper-case letters are used to indicate steady state quantities.

In terms of the d-q variables, the electromagnetic torque is identical to that of a synchronous machine, namely,

$$T_e = \frac{3}{2}\frac{P}{2}\left(\lambda_{ds} i_{qs} + \lambda_{qs} i_{ds}\right) \tag{3.21}$$

where P is the number of poles.

Using (3.12), the torque equation can be expressed by,

$$T_e = \left(\frac{3}{2}\right)\left(\frac{P}{2}\right)\left(\lambda_m i_{ds} + (L_d - L_q) i_{ds} i_{qs}\right) \qquad (3.22)$$

3.4 Operation of PMa-SynRM

In general, a current controlled inverter-fed PMa-SynRM should work in two modes. When the motor speed is lower than the rated speed or base speed, the motor drive is required to provide constant torque (rated torque). On the other hand, when the speed is greater than the rated speed, the load torque is inverse proportion with the speed. Figure 3-2 shows the torque/power vs. speed characteristics curve of the PMa-SynRM drive system. It can be seen that a large torque for starting and low-speed operation is required while the constant power over wide high-speed range preferred because it can significantly reduce the cost and size of the motor drive system.

The constant torque operation can easily be achieved by a PMa-SynRM motor as long as the inverter output voltage does not reach its limit. However, when the speed is above the rated speed, the back-EMF of the machine approaches the input source voltage so that the motor drive usually suffers from achieving its constant power operation. Recently, flux-weakening control has been developed to deal with this problem. By employing the field component of stator current to weaken the air-gap field produced by the permanent magnets, this approach allows the motor drive to extend the motor speed. This is known as flux-weakening control and thus the motor is operated in the flux-weakening region.

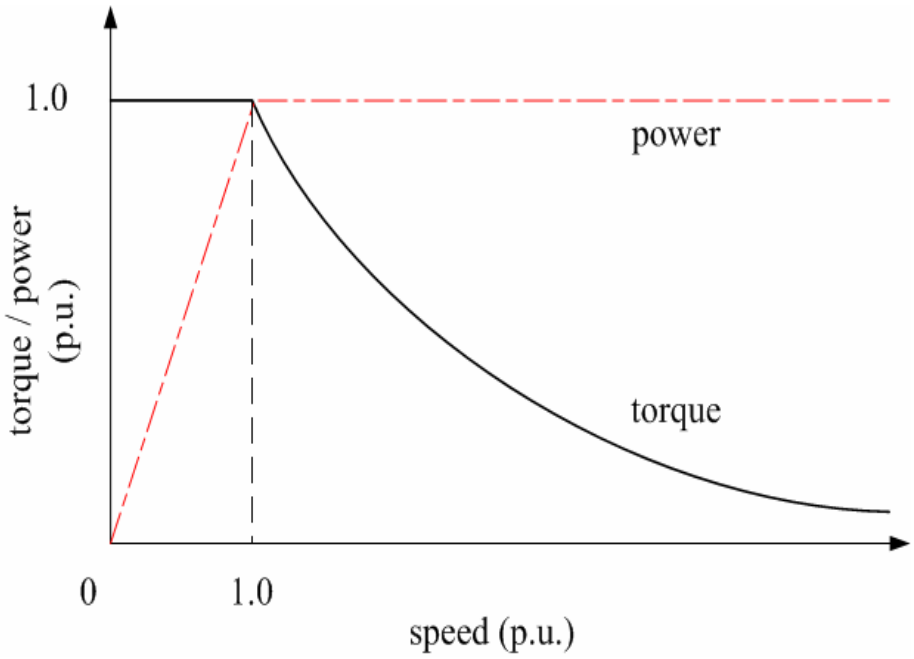

Figure 3-2 Torque/power Vs speed characteristics of PMa-SynRM

3.5 Vector Control of PMa-SynRM Machine

The term "vector control" is applied to those control techniques which have the ability to control both the amplitude and phase of the AC excitation of the machine. The vector control of currents and voltages results in control of spatial orientation of rotor and stator magnetic fields. Hence, it also is referred to as field oriented control.

The requirements necessary to control the torque production in a PMa-SynRM motor are (1) an independently controlled stator current to overcome the stator winding resistances, leakage inductances and induced voltage. (2) an independently controllable spatial angle γ as defined in the basic phasor diagram of the PMa-SynRM machine.

The instantaneous torque equation (3.22) defines a hyperbola in i_d-i_q plane for every value of torque. As a result, there exist infinite combinations of i_d and i_q which will deliver the same torque. Since the high efficiency is one of the important requirements of many high performance drives, the maximum torque per stator current is considered as the control criterion. The control criteria are also influenced by the voltage and current limit of the drive which can be explained with the help of the machine circle diagram.

3.5.1 Circle Diagram of Stator Current and Voltage

With voltage-fed inverter for PMa-SynRM, the dc bus is maintained as a stiff voltage by the use of large capacitors in the dc link. Therefore, the bus voltage of VSI is fixed or varies only within a small range. With the speed of the PMa-SynRM motor going up, the voltage applied to the motor must increase accordingly to counteract the speed-proportional induced back-EMF in the stator windings. When the speed reaches the rated value, eventually, the voltage applied to the PMa-SynRM cannot be further increased to maintain the current required for torque production. On the other hand, considering the current capability, the maximum stator current is limited by the current rating of the inverter as well as the thermal rating of stator windings. Therefore, the maximum output torque and power developed by PMa-SynRM is ultimately determined by the maximum current and voltage which inverter can apply to the machine.

Neglecting the ohmic voltage drop of stator resistance, the limit of the maximum stator voltage is expressed in terms of steady-state currents as

$$\left(\omega_r L_d I_{ds}\right)^2 + \left(-\omega_r L_q I_{qs} + \omega_r \lambda_m\right)^2 \le V_{s\max}^2 \qquad (3.23)$$

The above equation can be rearranged to form

$$\left(\frac{I_{ds}}{L_q / L_d}\right)^2 + \left(-I_{qs} + \frac{\lambda_m}{L_q}\right)^2 \le \left(\frac{V_{s\max}}{\omega_r L_q}\right)^2 \qquad (3.24)$$

$$\left(\frac{I_{ds}}{V_{s\max} / (\omega_r L_d)}\right)^2 + \left(\frac{-I_{qs} + \frac{\lambda_m}{L_q}}{V_{s\max} / (\omega_r L_q)}\right)^2 \le 1 \qquad (3.25)$$

For various speeds (3.24) or (3.25) produces a set of concentric ellipses in the i_d-i_q plane as plotted in the Figure 3-3. The center of these ellipses lies at the point $(0, \frac{\lambda_m}{L_q})$. The length of the major and minor half axes of the ellipses are $V_{s\max} / (\omega_r L_q)$ and $V_{s\max} / (\omega_r L_d)$, respectively.

As mentioned earlier, the current limit is decided by the continuous armature current rating and/or rating of the inverter switches. The current limit equation must satisfy

$$I_{qs}^2 + I_{ds}^2 \le I_{s\max}^2 \qquad (3.26)$$

where $I_{s\max}$ is the allowable maximum stator current.

It should be noted here that while plotting the circle diagram of the voltage and current limits, normally core loss, resistive drop and effect of the magnetic saturation over the machine parameters are neglected. Also, if the d-axis saturation effect is considered the voltage limit ellipses are distorted in horizontal direction and inclusion of

the resistive drop in the current and voltage limit equations shows noticeable counter clockwise tilt in the vertical direction of the ellipses.

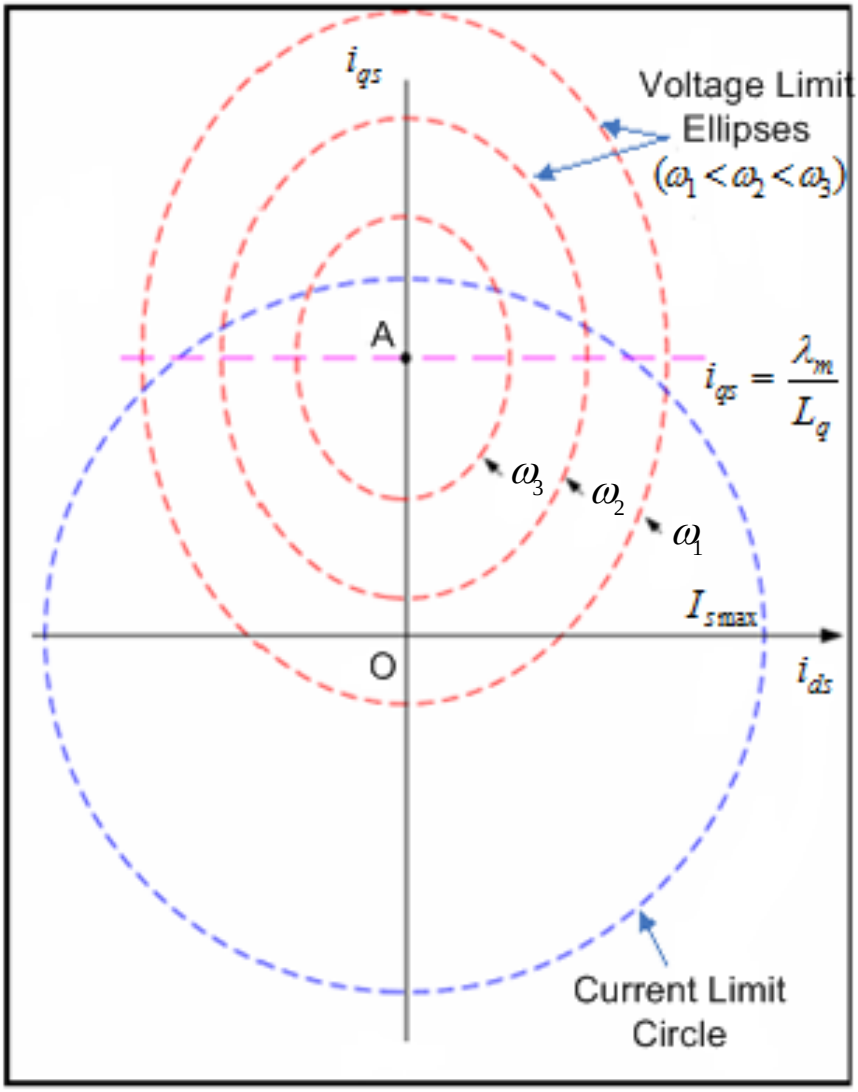

Figure 3-3 Current and voltage limits of PMa-SynRM

3.5.2 Current Trajectories

The torque equation (3.22) expressed in terms of the current angle γ is given by

$$T_e = \left(\frac{3}{2}\right)\left(\frac{P}{2}\right)\left(\lambda_m I_s \cos\gamma + \frac{1}{2}(L_d - L_q) I_s^2 \sin 2\gamma\right) \qquad (3.27)$$

It can be shown from (3.27) that maximum torque per ampere (MTPA) occurs at an optimum current angle which leads to the combination of optimum i_d and i_q values. By plotting these values in the i_d-i_q plane, the maximum torque per ampere (MTPA) trajectory of the Figure 3-4 can be obtained where the current and voltage limits diagram is shown. In the i_d-i_q plane, each value of the constant torque produces a hyperbola as shown in the Figure 3-4.

3.5.3 Control Principles

In order to satisfy current and voltage limits, the stator current must lie inside the current limit circle and voltage limit ellipse in all operating conditions. Therefore the control trajectories under the vector control are dictated by these limits.

There are a number of vector control schemes available and among them the rotor flux-oriented control scheme is relatively simple and practical and also has fast dynamics. The block diagram of the current control of the PMa-SynRM machine with rotor flux-orientation is shown in the Figure 3-5. For these motor drive applications, the reference i_d^* current is derived from a speed controller, position controller or torque controller and the reference i_q^* current is calculated from MTPA control algorithms depending on operating conditions. It is assumed that there is no phase lag of current regulation.

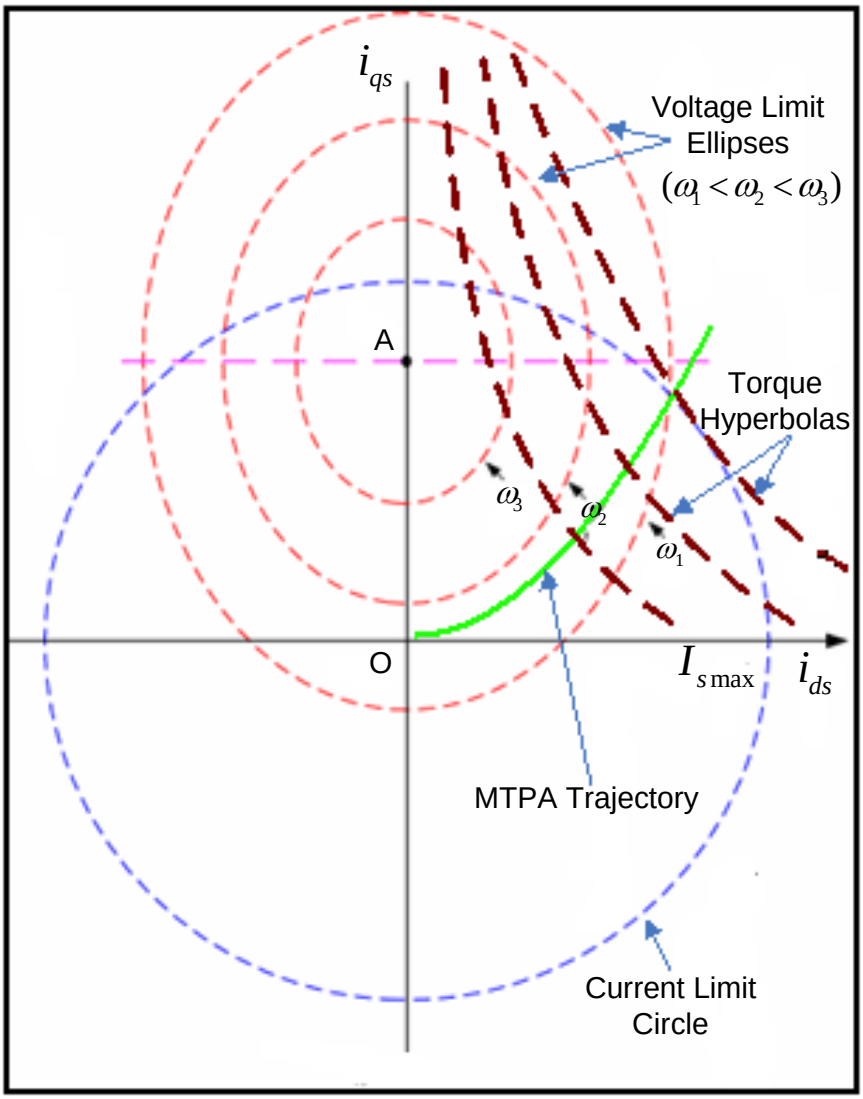

Figure 3-4 Current trajectories

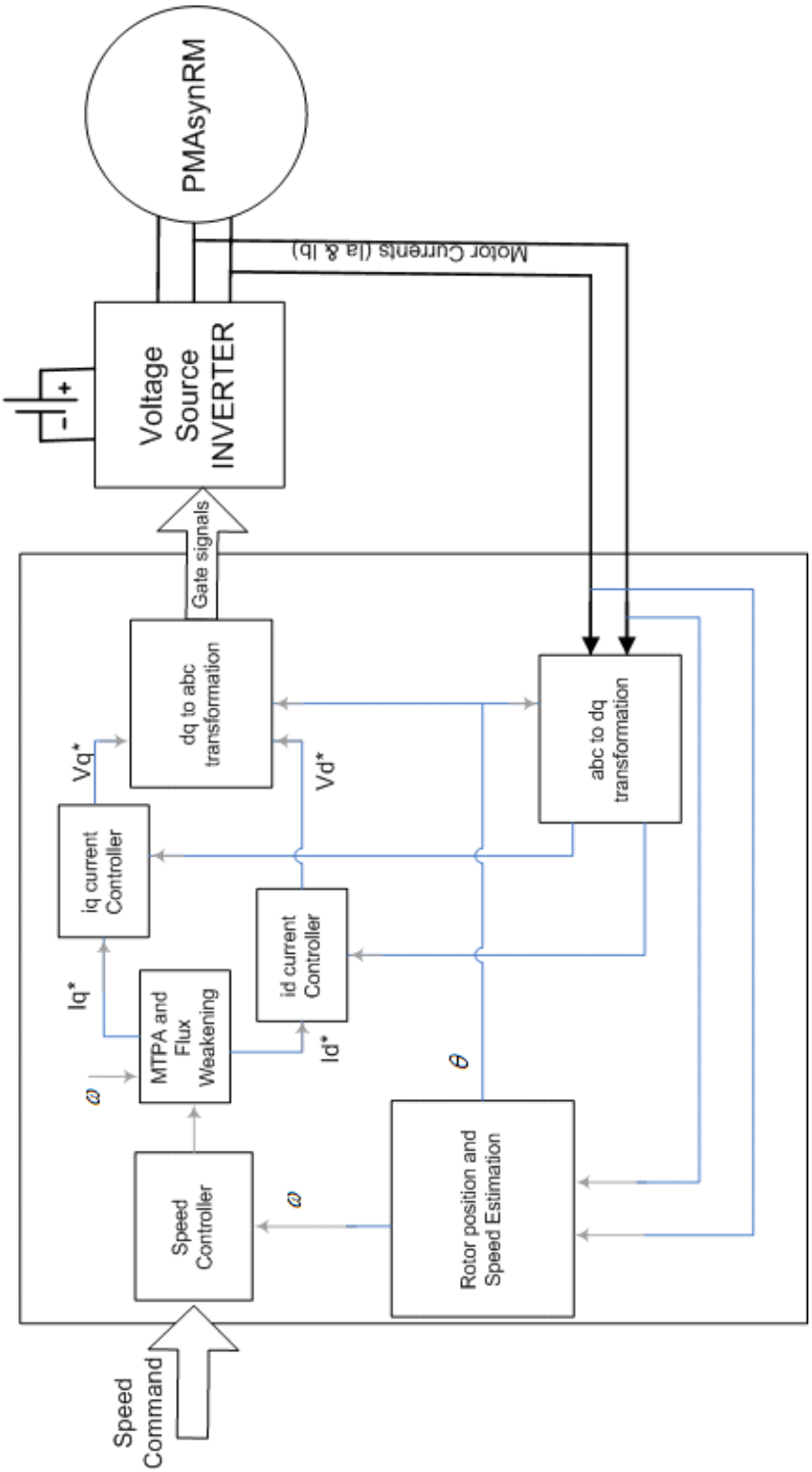

Figure 3-5 Block diagram of current vector control for motoring

According to (3.18) and (3.19), the steady-state phasor diagram shown in Figure 3-6 can be plotted. The phasor diagram shows constant-torque operation of PMa-SynRM motor using the MTPA strategy. The angle between the back-EMF and the stator voltage is the load angle δ, and the displacement angle of the stator current is ϕ.

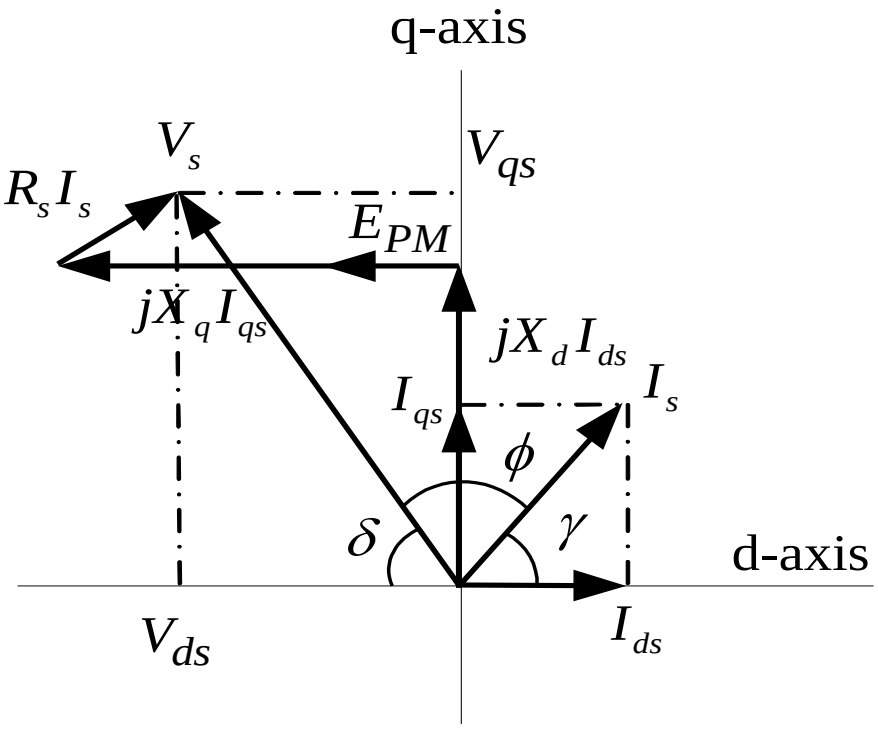

Figure 3-6 Steady-state phasor diagram of PMa-SynRM

3.5.4 Maximum Torque per Ampere Control (MTPA)

The optimal current phase angle at which the torque per current ampere becomes maximal is derived from (3.27) as follows.

$$\gamma = \sin^{-1}\left(\frac{-\lambda_m + \sqrt{\lambda_m^2 + 8(L_d - L_q)^2 I_s^2}}{4(L_d - L_q) I_s}\right) \qquad (3.28)$$

The relation between the d-axis and the q-axis currents for the maximum torque per ampere (MTPA) condition is given by,

$$i_q = \frac{\lambda_m}{2(L_d - L_q)} - \sqrt{\frac{\lambda_m^2}{4(L_d - L_q)^2} + i_d^2} \qquad (3.29)$$

Under the MTPA control, the PMa-SynRM is able to accelerate with maximum constant torque till the speed reaches a value at which the terminal voltage V_s reaches the limit value $V_{s\max}$. Thus the maximum speed under constant torque is given by,

$$\omega_b = \frac{V_{s\max}}{\sqrt{(\lambda_m - L_q i_q)^2 + (L_d i_d)^2}} \qquad (3.30)$$

This speed can also be called as the base speed or rated speed of the PMa-SynRM machine since; above this speed the machine needs to be operated with flux-weakening control.

3.5.5 Flux Weakening Control (FW)

As the stator voltage of the machine reaches its limit, the current vector needs to be controlled in such a way that it lies inside the voltage limit ellipse as shown in Figure 3-5. Considering the resistive drop of the system, the voltage limit value is defined as

$$V_{om} = V_{s\max} - I_{am} R \qquad (3.31)$$

The function of the flux weakening control is to control the d and q axis current in such a way that the voltage of the machine can be maintained at V_{om}. The optimum current vector producing the maximum torque at speed ω is derived from (3.23) and the condition of $I_a = I_{am}$,

$$i_q = \frac{-\lambda_m L_q + \sqrt{(\lambda_m L_q)^2 - (L_d^2 - L_q^2)\left\{\left(\frac{V_{om}}{\omega}\right)^2 - (L_d I_{am})^2\right\}}}{(L_d^2 - L_q^2)} \qquad (3.32)$$

$$i_d = \sqrt{I_{am}^2 - i_q^2} \qquad (3.33)$$

This current vector corresponds to the intersection point of the current limit circle and the voltage limit circle as shown in Figure 3-7 which corresponds to point ‘B’. The amplitude of the current vector is kept at the limiting value I_{am} and its phase angle increases as the speed increases till point ‘C’ in the figure. In this situation, the q-axis current increases towards positive direction and the d-axis current decreases as the speed increases maintaining constant power. Beyond point ‘C’, the flux-weakening range can be extended by using the voltage limited maximum output trajectory shown in the figure as path ‘CA’. The i_d and i_q relation should then follow the voltage limited maximum output control which is not discussed as part of this thesis.

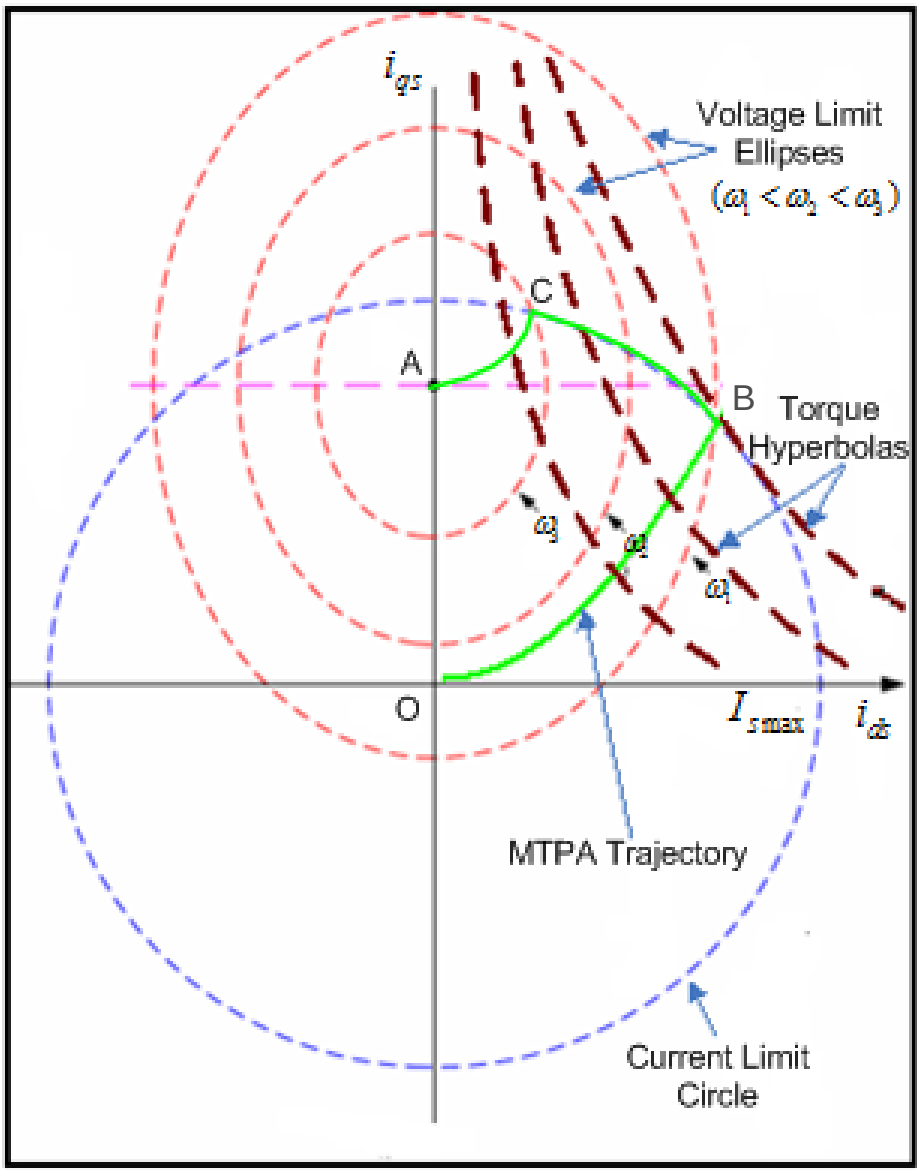

Figure 3-7 Current trajectories for MTPA and FW control modes

3.6 Parameter Measurement of PMa-SynRM Motor

The most common parameters used in the implementation of control algorithms are the simplified model parameters. These are

- R_a - Armature Resistance

- L_d - the direct axis self inductance
- L_q - the quadrature axis self inductance
- λ_m - the permanent magnet flux linkage

These parameters are used to calculate control rules discussed above such as voltage limit ellipses and maximum torque per ampere trajectories in vector control.

3.6.1 Armature Resistance (R_a) Measurement

The stator resistance of the motor can be easily measured from the standard DC measurement. Since R_a is the resistance between line-to-neutral, R_a will be one half of the measured line-to-line resistance.

3.6.2 Determination of Back EMF Constant (λ_m)

The back-EMF constant of a PMa-SynRM is determined from the open circuit phase voltage when it is driven by other motor. If the back-EMF is assumed to be sinusoidal, it is related to rotor speed and phase voltage as follows

$$V = \omega\lambda_m \qquad (3.34)$$

3.6.3 d-Axis Inductance Measurement (L_d)

Both static and dynamic measurements techniques can be used to measure the d-axis inductance L_d. For the static measurement of L_d, dc excitation is first applied between the B and C stator terminals to align the rotor q-axis with the stator MMF axis

as shown in Figure 3-8. Additional clamping may be necessary if the rotor angular position oscillates during ac excitation.

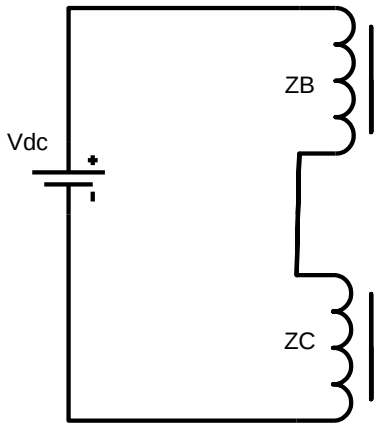

Figure 3-8(a) Alignment of the rotor q-axis with stator MMF axis

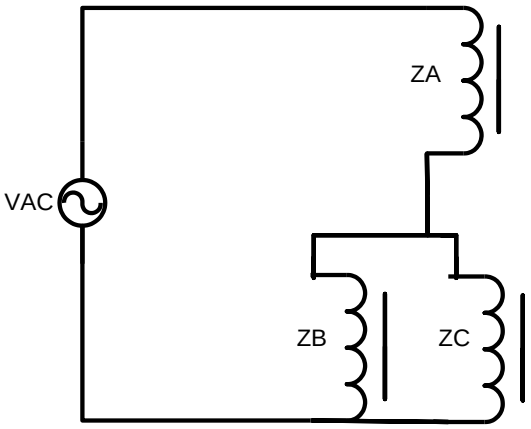

Figure 3-8(b) L_d measurement technique using ac excitation along rotor d-axis

Using a variac connected to 3 phase 60Hz supply, connect one terminal of the variac to both Phase B and Phase C terminals (Short Circuit Phase B and Phase C terminals) and the other terminal to Phase A of the stator windings as shown in the figure. Increase the voltage settings on the variac and at each incremental level, measure both the line voltage as well as the current. With the data collected, the d-axis inductance can be calculated as follows:

$$Z_A = \frac{\frac{2}{3}V_{LL}}{I_L} = \omega L_d \qquad (3.35)$$

where $\omega = 2\pi 60$ rad/sec

$$L_d = \frac{\frac{2}{3}V_{LL}}{\omega I_L} \tag{3.36}$$

3.6.4 q-Axis Inductance Measurement (L_q)

For the static measurement of the q-axis inductance (L_q), the rotor q-axis is first aligned with the stator d-axis (i.e., stator phase A axis) by using dc voltage to excite the stator winding as shown in Figure 3-9. The ac excitation is next applied along the rotor q-axis.

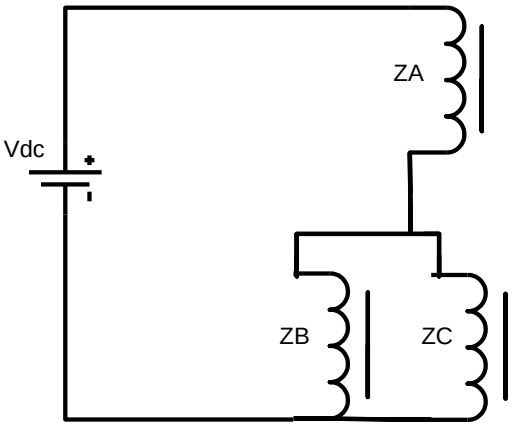

Figure 3-9(a) Alignment of the rotor d-axis with stator q-axis

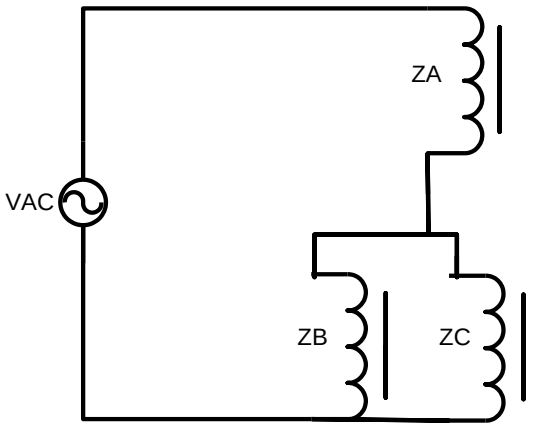

Figure 3-9(b) L_q measurement technique using ac excitation along rotor q-axis

Using a variac connected to 3 phase 60Hz supply, connect one terminal of the variac to both Phase B and Phase C terminals (Short Circuit Phase B and Phase C terminals) and the other terminal to Phase A of the stator windings as shown in the

figure. Increase the voltage settings on the variac and at each incremental level, measure both the line voltage as well as the current. With the data collected, the q-axis inductance can be calculated as follows:

$$Z_A = \frac{\frac{2}{3}V_{LL}}{I_L} = \omega L_q \qquad (3.37)$$

where $\omega = 2\pi 60$ rad/sec

$$L_q = \frac{\frac{2}{3}V_{LL}}{\omega I_L} \qquad (3.38)$$

3.7 Summary

In this chapter, mathematical models of PMa-SynRM are established in both, the stationary reference frame and the rotating reference frame. By using Park's transformation, all time varying inductances in the voltage equations are eliminated and in turn the models are simplified and vector control algorithms can be implemented.

Constant-torque and Constant-power operation is introduced in the PMa-SynRM drive system. After this, the voltage and current constraints imposed by both Voltage source inverter and motor itself are discussed.

Lastly, the vector control of PMa-SynRM machine, especially the Maximum Torque per Ampere (MTPA), and Flux-Weakening controls is reviewed. By using MTPA, the motor can operate with optimal efficiency at low speeds and using flux-weakening, the motor can operate beyond the rated speed. Also, parameters identification which is essential to implement the controls is discussed.

CHAPTER IV

ROTOR POSITION ESTIMATION FOR PMA-SYRNM

4.1 Introduction

This chapter will present a sliding mode observer technique for sensorless speed control of PMa-SynRM. The design of the sliding mode observer is based on the machine model in stationary reference frame derived in chapter III. The digital implementation of the sliding mode observer to PMa-SynRM motor is also presented.

4.2 Theoretical Fundamental of Sliding Mode Observer

In Sliding Mode Observer, the sliding problem is treated as a special case of a state controller problem. Thus, the sliding mode control is first discussed before explaining sliding mode observer.

Let a nonlinear system defined by differential equations in n-dimensional state space with m-dimensional control action be:

$$\dot{x} = f(x,t,u) \qquad (4.1)$$

Where $x \in R^n$ are the states and $u \in R^m$ is the control signal. Then, the design procedure of sliding mode consists of two steps. First, a sliding surface, $s(x; t) \in R^n$ is selected such that the desired system dynamics are achieved according to some performance criterion such as tracking, regulation and stability, when the system state trajectories are restricted to the sliding surface. Second, a discontinuous control law

u(x; t) is defined such that the states of the system reach the sliding surface and sliding mode exists on the surface.

A time varying sliding surface S(t) is first defined by the scalar equation $s(\tilde{x};t)=0$ with

$$s(\tilde{x};t)=(\frac{d}{dt}+\lambda)^{n-1}\tilde{x},\lambda>0 \qquad (4.2)$$

Where λ is a positive constant and $\tilde{x}$ = x - x_d is the tracking error vector. The problem of tracking x ≡ x_d is equivalent to force the state x of a plant remain on the surface S(t). When $s(\tilde{x};t)$ is greater than zero, the structure is varied such that the states, manipulated by control law, decrease $s(\tilde{x};t)$, and the opposite occurs when $s(\tilde{x};t)$ is less than zero. The sufficient condition for such positive invariance of S(t) is to choose the control law such that outside of S(t)

$$\frac{1}{2}\frac{d}{dt}s^2(\tilde{x};t)\le-\eta|S| \qquad (4.3)$$

Where η is a positive constant. The above inequality constrains trajectories to point towards the surface S(t) as shown in Figure 4-1. The surface S(t) is called the sliding surface, and the condition of control is known as the sliding condition.

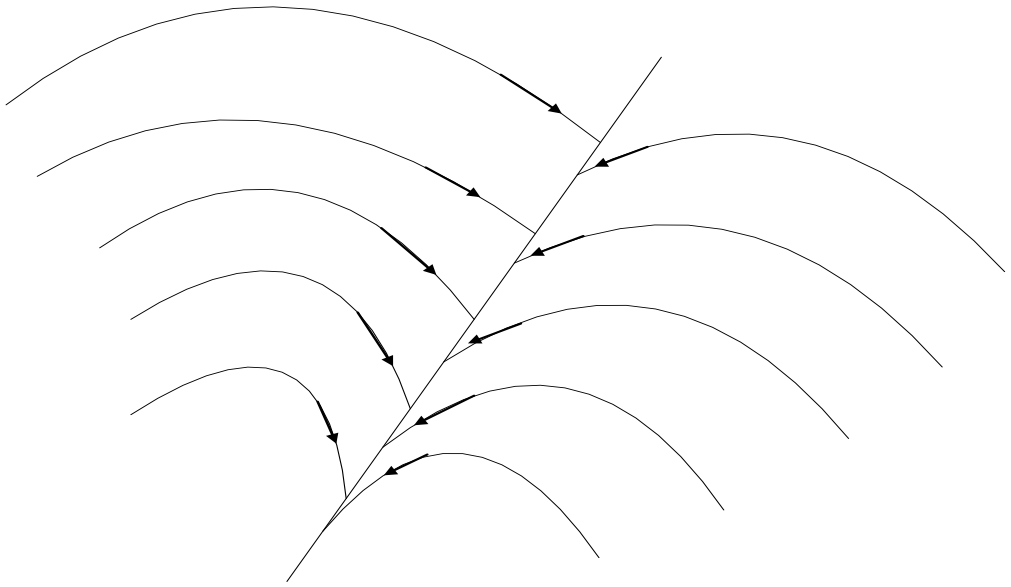

Figure 4-1 The sliding condition

The problem is similarly exploiting sliding behavior in the design of the observer, rather than controllers, is that the full state is not available for measurement, and the sliding surface definition is not adequate. Thus, in the design of the sliding mode observer, the sliding problem is treated as a special case of a state controlled problem, where the sliding surface are designed based on the error dynamics of the state variable estimates. The sliding surface is reached when the state estimation error goes to zero in a finite time and at the same time all other errors in the state estimates decay exponentially. Based on the above idea, the sliding mode observer of PMa-SynRM motor is developed in the next section.

4.3 Sliding Mode Current Observer of PMa-SynRM

The sliding mode observer is built based on the PMa-SynRM model in the stationary reference frame. The model in the stationary reference frame is characterized by:

$$\frac{d}{dt} i_s = A \cdot i_s + B \cdot v_s - B \cdot E_s \tag{4.4}$$

where $i_s = [\, i_{ds}^s \quad i_{qs}^s \,]$, $v_s = [\, v_{ds}^s \quad v_{qs}^s \,]$, $E_s = [\, e_{ds}^s \quad e_{qs}^s \,]$

$$A = (-r_s / L_s) \cdot I \tag{4.5}$$

$$B = (1 / L_s) \cdot I \tag{4.6}$$

$$\begin{cases} e_{ds}^s = K_e \omega_r \cos\theta_r \\ e_{qs}^s = K_e \omega_r \sin\theta_r \end{cases} \tag{4.7}$$

From (4.4), the sliding mode observer is defined as:

$$\frac{d}{dt} \hat{i}_s = A \cdot \hat{i}_s + B \cdot (v_s - K_s \cdot \mathrm{sgn}(S)) \tag{4.8}$$

Where S is the stator current error and K_s is the gain matrix.

$$K_s = k_s \cdot I \tag{4.9}$$

$$S = [s1 \;\; s2]^T = \hat{i}_s - i_s \tag{4.10}$$

The sliding surface is defined upon the stator current errors and is given by,

$$e_s = \hat{i}_s - i_s = 0 \tag{4.11}$$

The estimation error dynamic is given by the following equation,

$$\dot{S} = \frac{d}{dt}(\hat{i}_s - i_s) = A \cdot (\hat{i}_s - i_s) + B \cdot (E_s - K_s \cdot \mathrm{sgn}(S)) \tag{4.12}$$

The above dynamic function is disturbed by the unknown induced EMF components. In order to guarantee that the sliding surface is achieved, Lyapunov function is used. The Lyapunov function V is chosen as:

$$V = \frac{1}{2} S^T S \tag{4.13}$$

Under the assumption that the rotor speed is constant within one estimated period, the derivative of Lyapunov function becomes:

$$\dot{V} = S^T \cdot \dot{S} = S^T [A \cdot S + B \cdot (E - K_s \cdot \text{sgn}(S))] \tag{4.14}$$

According to Lyapunov's stability theory, $\dot{V}$ must be negative to ensure that the observer is stable. Since parameter A is negative, and back-EMF component is bounded, the sliding surface is reached after a finite time interval if the sliding gain satisfies

$$K_s > |E| \tag{4.15}$$

4.3.1 Position Estimation

After the sliding surface is reached, comparing (4.4) and (4.8), the sliding component $K_s \cdot \text{sgn}(S)$ is the back-emf with some high frequency harmonics. It may not be suitable to estimate the rotor position, so a low pass filter is needed to smooth the back-emf. It is noted that the electrical time constant is much smaller than the mechanical time constant, especially for high-pole machines. Therefore, it is reasonable to assume that the machine speed is constant over a short time interval. Hence, the dynamics of the back-emf can be described as:

$$\frac{d}{dt}\begin{bmatrix} e_{qs}^s \\ e_{ds}^s \end{bmatrix} = \begin{bmatrix} 0 & -\omega_r \\ \omega_r & 0 \end{bmatrix} \begin{bmatrix} e_{qs}^s \\ e_{ds}^s \end{bmatrix} \tag{4.16}$$

thus the filter can be defined as :

$$\frac{d}{dt}\begin{bmatrix} \hat{e}_{qs}^s \\ \hat{e}_{ds}^s \end{bmatrix} = \begin{bmatrix} 0 & -\omega_r \\ \omega_r & 0 \end{bmatrix} \begin{bmatrix} \hat{e}_{qs}^s \\ \hat{e}_{ds}^s \end{bmatrix} - K_f \left(\begin{bmatrix} \hat{e}_{qs}^s \\ \hat{e}_{ds}^s \end{bmatrix} - K_s \cdot \mathrm{sgn}(S) \begin{bmatrix} 1 \\ 1 \end{bmatrix} \right) \tag{4.17}$$

The above filter has the structure of a Kalman filter and is expected to have high filtering properties. Cut-off frequency K_f varies according to the rotor speed.

After a smooth back-emf is obtained, the rotor angle can be calculated by:

$$\theta_r = \tan^{-1} \left| \frac{e_{qs}^s}{e_{ds}^s} \right| \tag{4.18}$$

the sign of the e_{ds}^s and e_{qs}^s decides the 4 quadrant of rotor angle. If e_{ds}^s is equal to zero,

$$\theta_r = \begin{cases} \pi/2, & e_{qs}^s > 0 \\ 3\pi/2, & e_{qs}^s < 0 \end{cases} \tag{4.19}$$

The rotor speed can be simply obtained from the derivative of the position.

4.4 Digital Implementation of Sliding Mode Current Observer

The position and speed estimator is based on a current observer as explained in the above section. So the digitized model of the motor can be represented as:

$$i_s(n+1) = (1 - T_s \cdot \frac{R}{L}) i_s(n) + \frac{T_s}{L}(v_s(n) - e_s(n)) \tag{4.20}$$

where

i_s = Motor current vector

v_s = Input voltage vector

e_s = back-EMF vector

R = Phase resistance

L = Phase inductance

T_s = Control cycle period

The digitized model is implemented in the software. In order to compensate the model, we make use of the closed loop feedback involving currents from model and from actual motor as shown in Figure 4-2. The closed loop involves calculation of the sign of the error between measured current and estimated current. The computed sign of the error is multiplied by the sliding mode controller gain (K). The output of this is the correction factor (Z) which is added to the voltage term from the digitized model and this process repeats every control cycle.

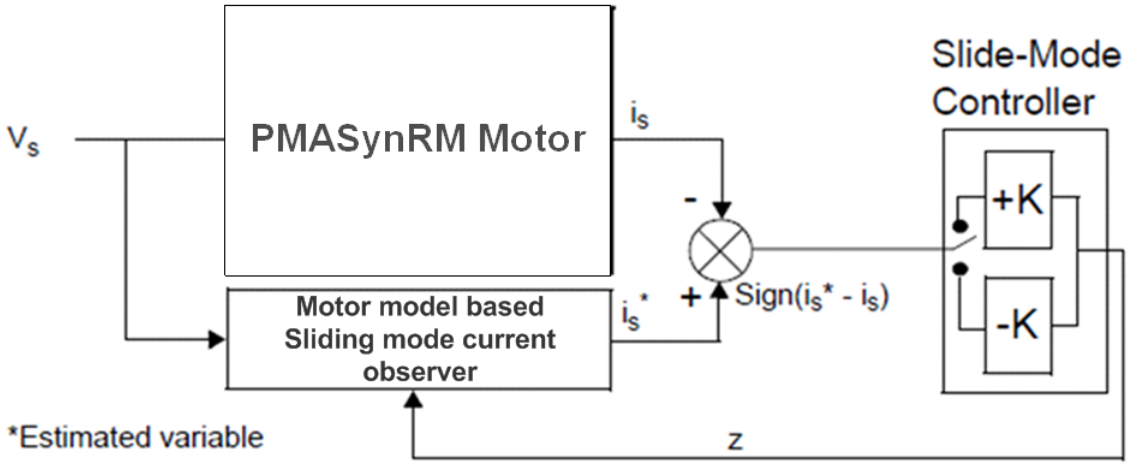

Figure 4-2 Sliding mode current observer

With the matching of measured currents (i_s) and estimated currents (i_s*), the estimated back-EMF (e_s*) is assumed to be the same as the actual back-EMF (e_s).

Once the digitized model is compensated, the next step is to estimate the back-EMF (e_s*) by filtering the correction factor (Z), as shown in Figure 4-3. The back-EMF estimation (e_s*) is fed back to the model to update the variable e_s* after every control cycle. Values e_{ds}^s and e_{qs}^s, vector components of e_s, are used for the estimated theta calculation. From the obtained theta values, the speed of the motor is then calculated.

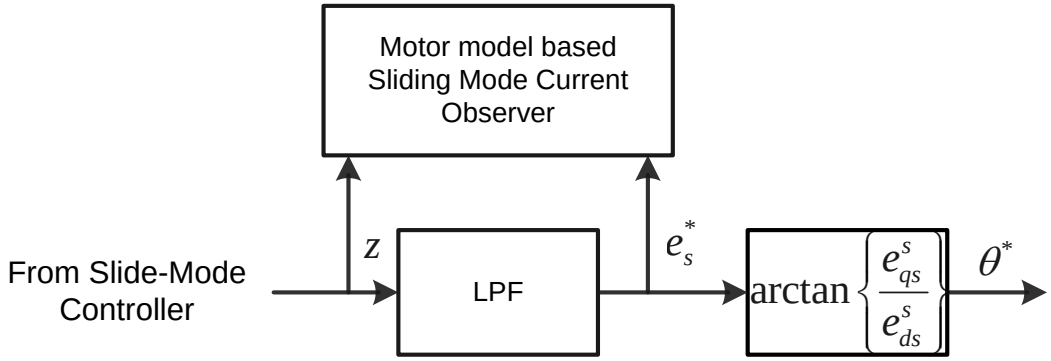

Figure 4-3 Back-emf estimation and theta calculation

With the proposed sensorless observer control, the motor suffers from starting due to a minimum speed is needed to get the estimated back-emf. So the motor on start-up is made to operate in open loop at a fixed acceleration rate while the FOC controls the current I_d and I_q. Once the motor attains the speed, close to 10% of the rated speed, the operation switches to the closed loop, sensorless control deriving the position and speed from position/speed estimator.

4.5 Sliding Mode Observer based Control of PMa-SynRM

Figure 4-4 shows the block diagram of the overall Sliding Mode Observer based speed control of PMa-SynRM drive system, which consists of the speed PI regulator, MTPA controller, two current PI regulators in the synchronous reference frame, a rotor position estimator by sliding mode observer and hence the speed calculation. In addition, the modules for Park transformations, space vector PWM generation module, and a three- phase inverter are shown with the PMa-SynRM motor.

As mentioned before, the motor suffers from starting due to the back-EMF of the PMa-SynRM is too small to be estimated accurately. Therefore, an open-loop starting algorithm with a ramp speed profile is designed to start the motor from standstill, up to a specified speed around 10% of the rated rpm, at which the sliding mode observer becomes active in the loop.

4.6 Summary

A sliding mode observer for position-sensorless control of PMa-SynRM has been developed. A concept of feedback equivalent control is introduced. Then, the digital implemenation of the Sliding mode observer for the PMa-SynRM control drive system is discussed.

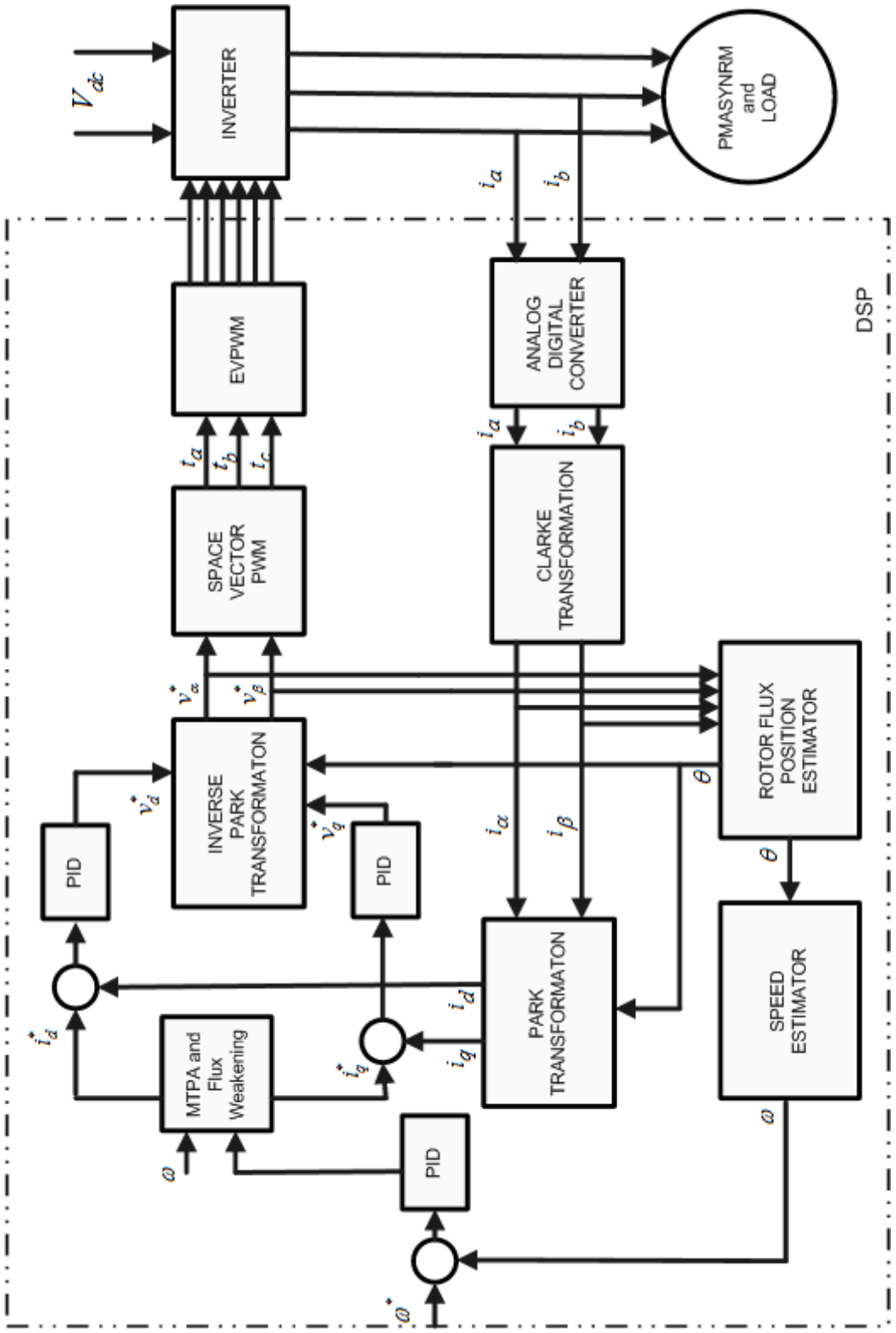

Figure 4-4 Block diagram of sensorless PMa-SynRM drive system using SMO

CHAPTER V

SYSTEM IMPLEMENTATION

5.1 Introduction

Experimental tests have been performed on a prototype PMa-SynRM drive system which consists of: 1) a three-phase IGBT power inverter connected to a DC power supply of 300V; 2) a digital controller based on an eZdspF2812 board with Texas Instruments TMS320F2812 DSP; 3) a dynamo setup as the load consisting of a DC generator connected to a resistive bank; and 4) a PMa-SynRM motor coupled with a dynamo and torque sensor.

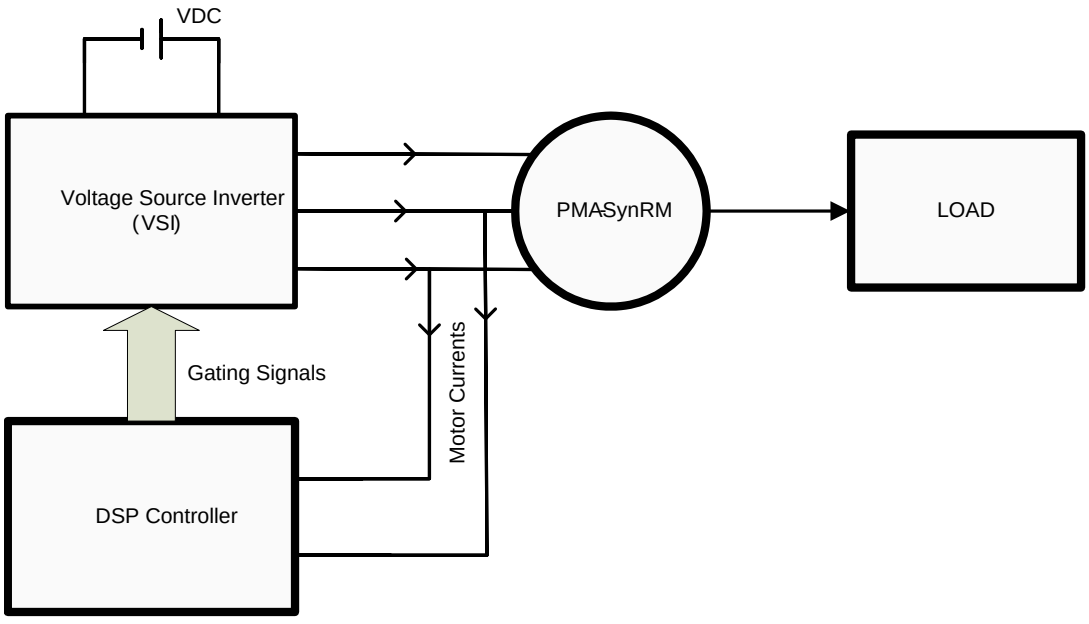

Figure 5-1 PMa-SynRM motor drive system

5.2 Experimental Setup

Experiments have been implemented on the 380W, 24 rotor poles and double barriers, 36 stator slots PMa-synRM motor with the concentrated windings as shown in Figure 5-2. The motor phases are star connected forming a floating neutral connection and an optical sensor disc are arranged on the stator. The back-EMF of this motor is nearly a sinusoidal wave as shown in Figure 5-3. The motor parameters are listed in Appendix A.

Figure 5-4 shows the experimental setup for the PMa-SynRM motor drive. The insulated gate bipolar transistors (IGBTs) are used as switching devices of the inverter. The switching frequency is set at $20\,kHz$ in this experiment. The digital controller carries out speed range control algorithms and drives the inverter to generate the applied three-phase voltage. Both of them are shown in Figure 5-5. A dynamo setup coupled to the motor as shown in Figure 5-6 is used to load the machine for rated torque of 28N-m. The measurement instruments are shown in Figure 5-7.

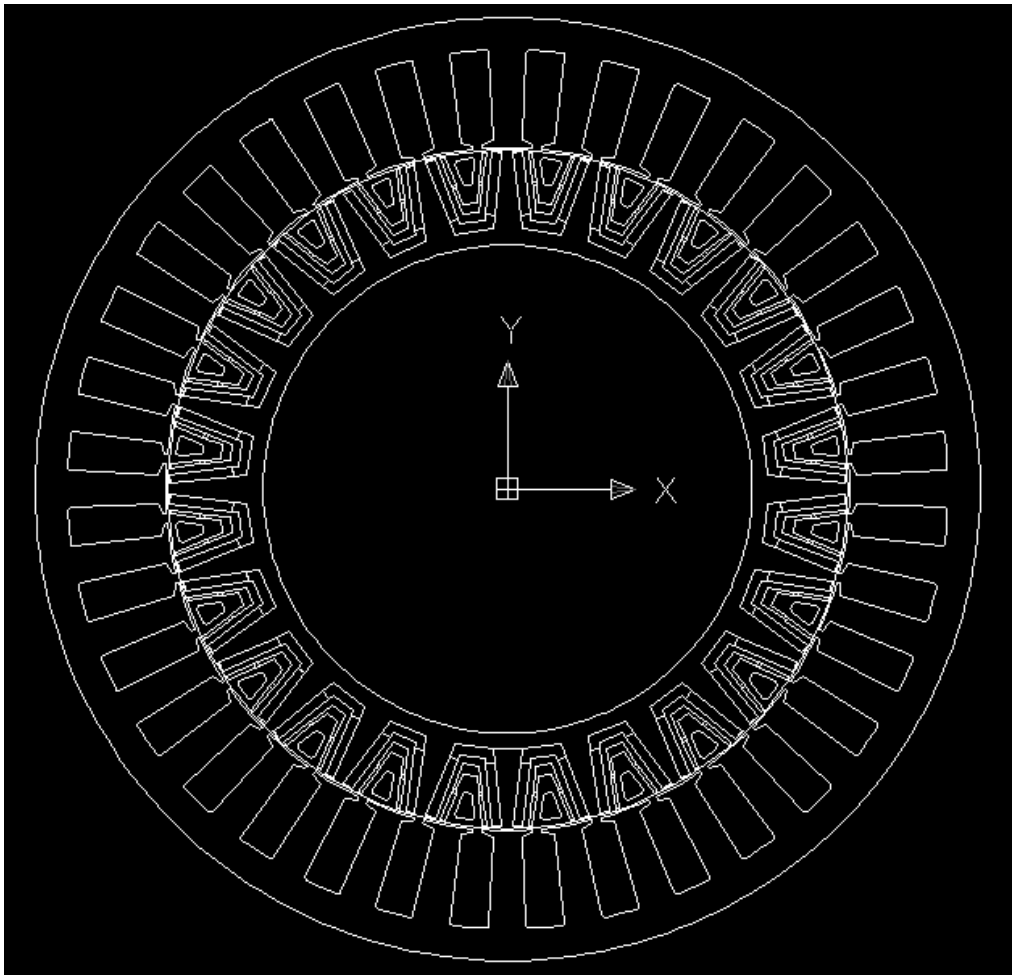

Figure 5-2 PMa-SynRM motor with 36 slots, 24 poles and double barriers

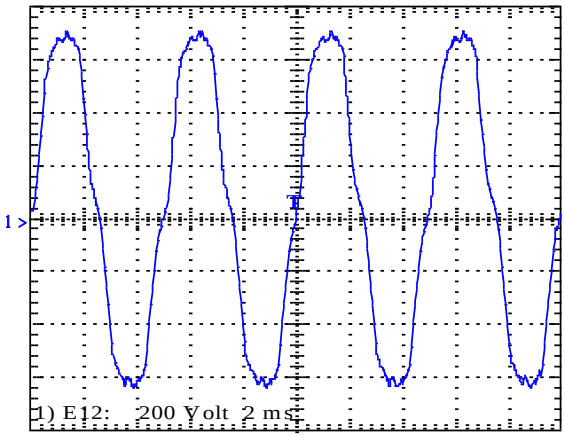

Frequency	201 Hz
Peak to Peak	1.34 kV
Maximum	704 V
Minimum	-640 V
AC RMS	489 V
Cycle AC RMS	491 V

Figure 5-3 Line-to-Line back-EMF waveform [Speed: 1000RPM, Temp: 21.1°C]

Figure 5-4 Experimental setup of the PMa-SynRM motor drive system

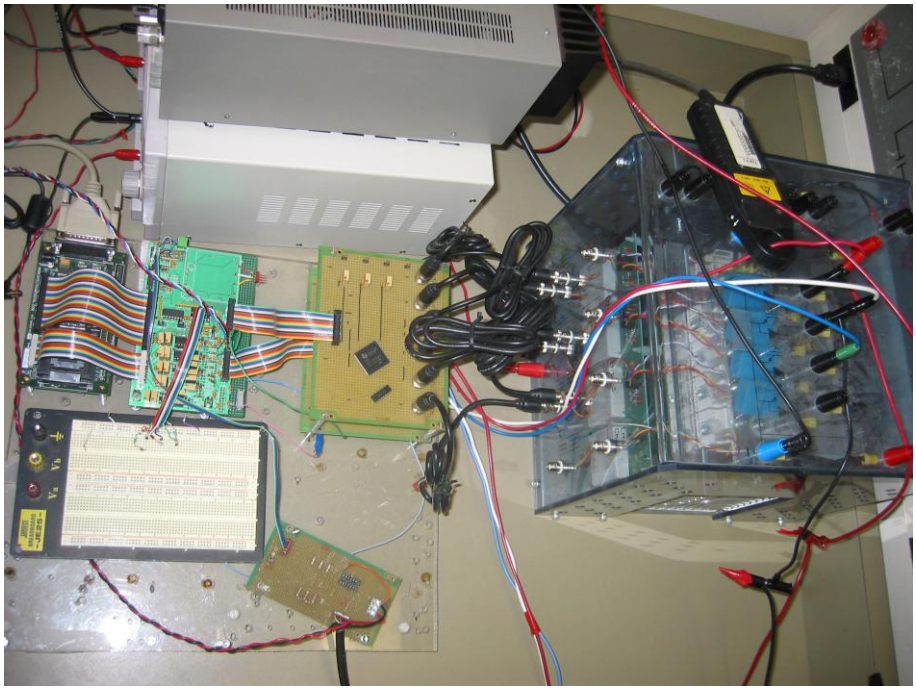

Figure 5-5 TMS320F2812 based controller and Inverter

Figure 5-6 PMa-SynRM motor (left) and dynamo load (right) setup

Figure 5-7 Instruments used for measurements

5.3 Hardware Setup of the Control System

The hardware structure of the control system is mainly composed of two interconnected modules: TMS320F2812 eZdsp and interface drive board. The controller reads the feedback currents, implements the speed control algorithm and finally generates the required six PWM gating signals to drive the PMa-SynRM motor.

TMS320F2812 has a 12-bit Analog-to-Digital Converter (ADC) with 8 or 16 multiplexed input channel, which transfer the 0~3V analog signal to 0000h-0FFFh digital signal. For every conversion, any of the available 16 input channels can be selected through the analog multiplexer. After the conversion is completed, the digital

value of the selected channel is stored in the appropriate result register (ADCRESULTn). The start of conversion can be synchronized with a trigger generated by event managers.

ADCIN0 and ADCIN1 are selected to be input channels of current sensing in the experiment. The trigger to start conversion is timer underflow interrupt. This function filters the switch frequency when the phase current is read.

Most of the software parameters are made available as signals using the PWMDAC which can then be captured on the oscilloscope in real time. This module converts any software variables with Q15 representation into the PWM signals in EVB for x281x by means of calculation the (full) compare values using Timer 3 for generating PWM outputs. The PWMx (x=7, 9, 11) are used for this purpose. An external low-pass filter is necessary to view the actual signal waveforms to filter out the high frequency component embedded in the actual low frequency signals. The range of the output signal waveforms is 0-3.3V. This feature is very useful during development stage for real time debugging and verification of the software.

5.3.1 Analog Signal Measurement

The current sensor outputs need to be rearranged and scaled so that it can be used by the control software. Therefore, the gain of signal conditioner and offset are adjusted to make the TMS320F2812 DSP read the signal correctly. Figure 5-8 shows the signal conditioning circuit where the offset is adjusted with K20 and the gain is adjusted with K14.

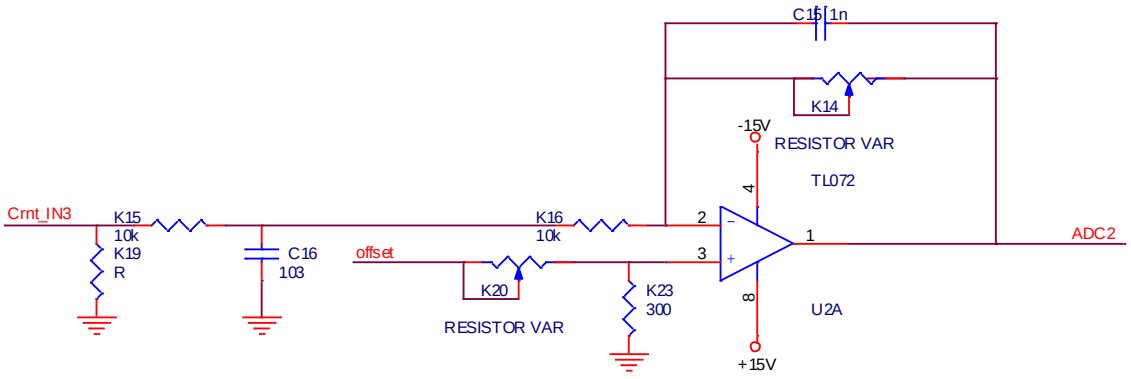

Figure 5-8 ADC input signal conditioning circuit

The ADCIN0 and ADCIN1 pins accepts the analog current sensor signals in the range of 0-3 volts with ground referenced to 0V (VREFLO = 0). Consequently, before connecting these signals to ADCINx pins, the hardware adjustment by external op-amp circuits (for gain and offset adjustments) for these analog signals such that they represent according to the selected base quantities and the appropriate voltage range is required.

5.4 Voltage Source Inverter (VSI)

A standard arrangement of an inverter circuit with six switches and the six freewheeling diodes is shown in Figure 5-9. At any given instant, both switches in one leg cannot be ON, as that would constitute a short circuit. Also, both switches cannot be OFF as that would leave an open circuit condition and the voltage would be unknown to the control system. Hence, the inverter has to be controlled in such a way that either the upper switch is ON while the lower switch is OFF and vice versa.

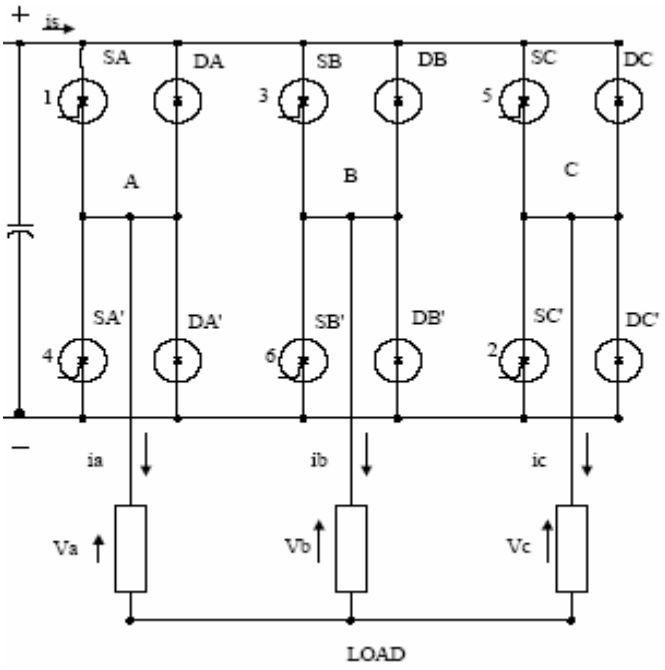

Figure 5-9 VSI with six switches and six free-wheeling diodes

The circuit operation is as follows. For example, SA is ON and i_a is positive, the current flows from the positive bus through SA to the load. When SA is OFF, and SA' is ON, the current flows from the negative bus and through the DA' as the inductive nature of the load impedance prevents the current from rapid change in direction which would allow it to flow through a newly turned 'ON' switch SA'.

Again, negative current in phase A can flow through SA' in 'ON' state, or through DA when SA' is OFF. Therefore, the current flowing to either switch is associated with the flow of electric power from supply source to load, while current flowing through either of the freewheeling diodes is associated with the flow of power in opposite direction to capacitor in the dc link.

5.4.1 Space Vector Pulse Width Modulation

The Space Vector PWM (SVPWM) technique is the most preferred PWM scheme for motor drives. Inverter voltage control by space vector modulation technique includes switching between the two active and zero voltage vector so that the time average within each switching cycle is equal to the voltage command. By simple digital calculation of the switching time one can easily implement the SVPWM scheme. There is no unique switching scheme, as the scheme has to be developed according to the choice of vectors.

5.4.2 Switching Logic

Only eight logic states are permitted for switching including two zero states. The switching assignments for the legs a, b, and c of the inverter are given below.

a = 0 if SA is OFF and SA' is ON
1 if SA is ON and SA' is OFF

b = 0 if SB is OFF and SB' is ON
1 if SB is ON and SB' is OFF

c = 0 if SC is OFF and SC' is ON
1 if SC is ON and SC' is OFF

The instantaneous line-to-line output voltages are then:

$$v_{ab} = v_{dc}(a-b)$$

$$v_{bc} = v_{dc}(b-c)$$

$$v_{ca} = v_{dc}(c-a)$$

where v_{dc} is the dc supply voltage of the inverter. The line-to-neutral voltages are then given by:

$$v_a = \frac{1}{3}(v_{ab} - v_{ca})$$

$$v_b = \frac{1}{3}(v_{bc} - v_{ab})$$

$$v_c = \frac{1}{3}(v_{ca} - v_{bc})$$

Substituting the values of v_{ab}, v_{bc} and v_{ca} in above equations, we get

$$v_a = \frac{v_{dc}}{3}(2a - b - c)$$

$$v_b = \frac{v_{dc}}{3}(2b - c - a)$$

$$v_c = \frac{v_{dc}}{3}(2c - a - b)$$

Therefore, from these equations we can see that the line-to-line voltages can only be either $-v_{dc}$, or v_{dc}. Whereas, the line-to-neutral voltages can be $-2/3\, v_{dc}$, $-1/3\, v_{dc}$, 0, $2/3\, v_{dc}$, $1/3\, v_{dc}$ depending on whether a, b and c are 0 or 1. We therefore get eight logic states from 0 to 7. Table 5-1 given below shows all the possible logic states and the corresponding voltages.

Table 5-1 Logic states and the corresponding voltages for the VSI

States	***A***	***b***	***c***	V_{ab}	V_{bc}	V_{ca}	V_a	V_b	V_c
Zero	0	0	0	0	0	0	0	0	0
V_1	0	0	1	0	-1	1	-1/3	-1/3	2/3
V_2	0	1	0	-1	1	0	-1/3	2/3	-1/3
V_3	0	1	1	-1	0	1	-2/3	1/3	1/3
V_4	1	0	0	1	0	-1	2/3	-1/3	-1/3
V_5	1	0	1	1	-1	0	1/3	-2/3	1/3
V_6	1	1	0	0	1	-1	1/3	1/3	-2/3
Zero	1	1	1	0	0	0	0	0	0

5.5 Software Development of PMa-SynRM Control System

The DSP-based software, implemented in C language, provides the control for the PMa-SynRM motor drive system. During the development, the hardware structures and its specific features are considered in order to achieve high processing speed and precision in the overall control system.

The total control software consists of two main modules, the initializing module and the PWM Interrupt Service Routine (INT2) module. The first one is executed only onetime at the startup to perform initializations for the program variables and peripherals, and configures the DSP for specific tasks, etc. The second module interrupts waiting loop by the PWM timer underflow. When the interrupt flag is set, the corresponding Interrupt Service Routine (ISR) is served.

The flowchart of the overall control system is shown in Figure 5-10:

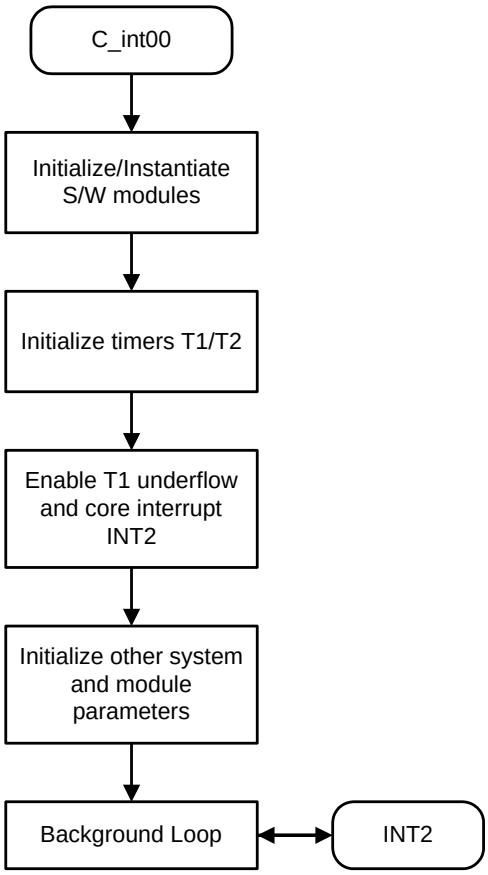

Figure 5-10 Flowchart of the PMa-SynRM control software

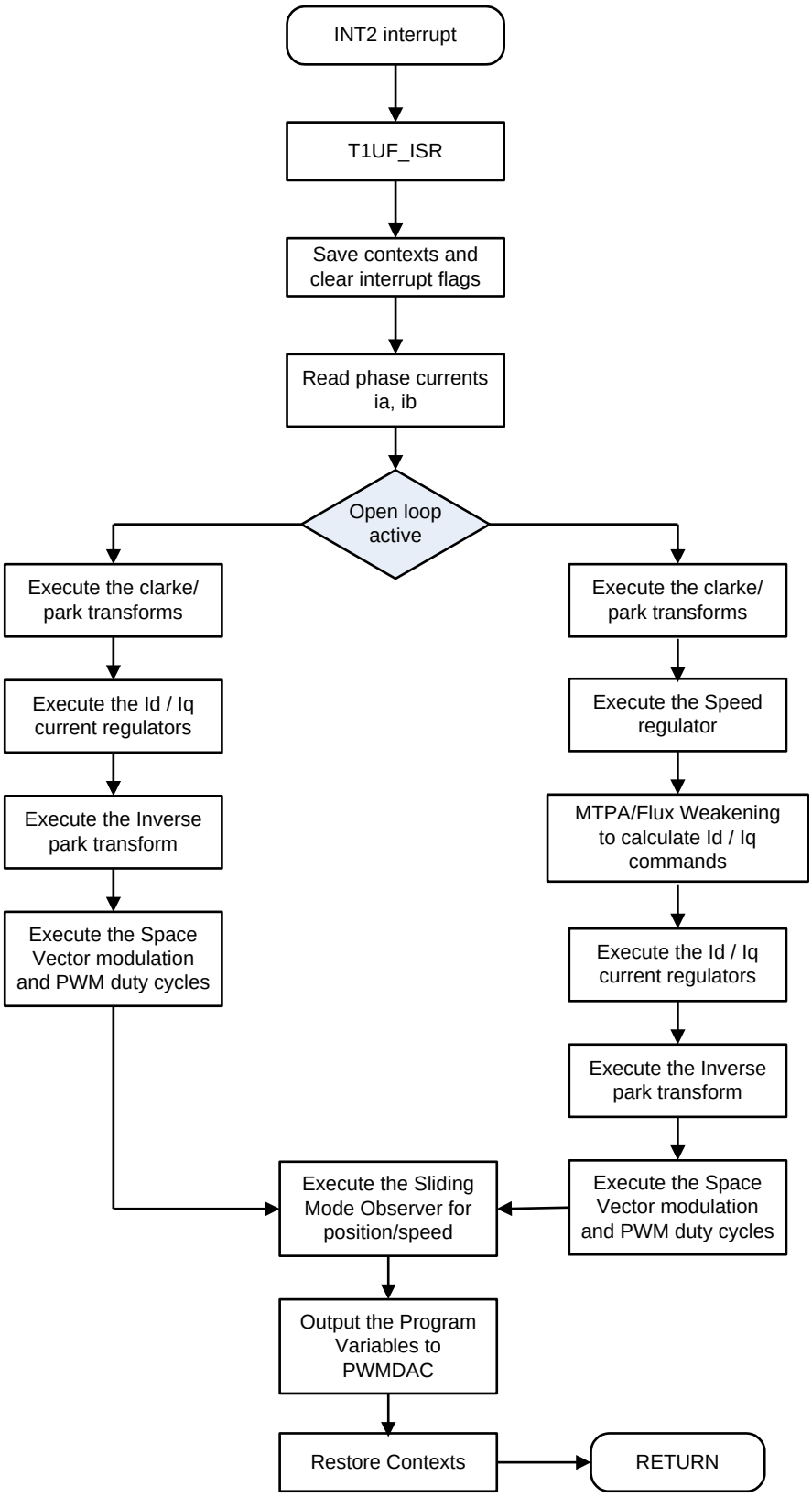

Figure 5-10 Cont.

5.5.1 Floating Point Arithmetic and Optimization

The software uses TI supplied IQ math library to perform floating-point arithmetic operations. The TMS320C28x IQmath Library is a collection of highly optimized and high precision mathematical functions for C/C++ programming to seamlessly port a floating-point algorithm into fixed-point code on TMS320C28x devices. These routines are used in computations required for software algorithms such as the PI controller, SVM, Park, Clarke and other functions where arithmetic operations are involved. By using these routines faster execution speed can be achieved.

The IQmath library functions occupy 360 bytes of memory. IQmath look-up tables occupy 6Kb memory stored in the Boot ROM. The detailed memory map of IQmath look-up tables is shown below in Table 5-2.

Table 5-2 IQmath look-up tables

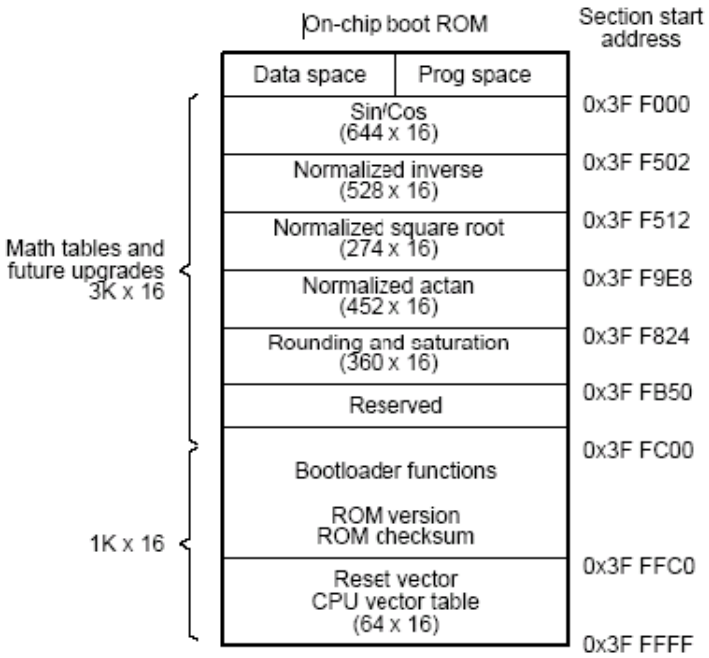

5.5.2 Base Values and Per-Unit Model

It is often convenient to express machine parameters and variables as per-unit quantities. Moreover, the TMS320F2812 is a fixed point DSP, so using a per-unit model of the motor is easier than using real parameters. However, IQ Math format used in "C" framework allows user employ the real parameters with quite high precision. In this model, all quantities refer to the base values. Base power and base voltage are selected and all parameters and variables are normalized using these base quantities. Although, we will violate this convention from time to time when dealing with instantaneous quantities, the rms value of the rated phase voltage and current are generally selected as base voltage for the abc variables while the peak value is generally selected as base voltage for the d-q variables.

The choice of maximum line current depends on the maximum motor current. This motor current again depends on multiple factors such as, motor drive ratings and load characteristics. In order to guarantee that the line current does not exceed the chosen maximum, a judgment factor can be applied to the selection. For example, if the maximum current is determined as 10A, then the line current can be normalized with a maximum value of 12A. The tradeoff of this large judgment factor is reduced resolution.

5.6 Experimental Result Analysis

A large number of experiments were conducted to verify the basic operation and performance characteristics of the motor drive system. The details of the experiments along with typical waveforms observed are reported in this section.

Figure 5-11 shows the Speed response of the system when the speed command changes from 0 to 130RPM (0.39 pu) and Phase A current (pu) as seen by DSP. The same plots are shown in Figure 5-12 with vertical cursors capturing the open loop time period. Figure 5-13 shows Phase A and Phase B currents (in pu) when the speed command changes from 0 to 130RPM (0.39 pu). The zoom portion shows the Phase B current lags Phase A by 120^0. Figure 5-14 shows the correctness of sliding mode observer estimated position. This position agrees with the position from the optical sensor. Both the position plots shown in the Figure 5-14 are in per unit. Figure 5-15 shows the plots of Phase A current (in pu), motor speed and sliding mode observer estimated position when the speed command is changed from 130RPM to 10RPM and then switched back to 130RPM. This indicates the robust speed control of the system and also the low speed operation. Figure 5-16 and Figure 5-17 shows plots of Phase A current, q-axis current and d-axis currents in pu during motor start and when the motor speed changes from 130RPM to 10RPM and back to 130RPM respectively. Figure 5-18 shows plots of Phase A current, speed command and motor speed in pu during the dynamo load changes. The next Figure 5-19 shows the same above plots in addition to Motor Phase A current from the current probe. Figure 5-20 and Figure 5-21 shows plots of Motor Phase A current from the current probe, q-axis and d-axis current for Id zero control and MTPA control respectively. The plots indicate that MTPA control is efficient and achieves the same torque for less current as compared to Id Zero control. The working of sliding mode observer in estimating the back-emfs and hence the position is verified from the Figures 5-22 and 5-23. Figure 5-22 shows Motor Phase A

current from the current probe, stationary frame estimated back-emfs (pu) and estimated position (pu) from the sliding mode observer whereas the Figure 5-23 shows actual and estimated currents instead of the back-emfs. As seen, the estimated back-EMF waveforms of e_{ds}^{s} and e_{qs}^{s} are so sinusoidal that the rotor position angle can be calculated accurately. Also, the estimated currents trace the sampled ones with minor errors according to the current level. Next, the reverse operation of the motor drive system is shown in Figures 5-24, 5-25 and 5-26. The robustness of the speed control is verified by changing the motor speed from -130 RPM to -10RPM and back -130RPM under full load condition of approximately 25N-m. The forward and reverse operation of the motor drive system is shown in the following Figures 5-27, 5-28 and 5-29. As the current starting process is an open loop start, the motor system when changing from forward to reverse has to first bring the motor to zero speed and then apply the open loop start and close loop accordingly. So, the speed command in the plots show zero speed till the actual motor speed decelerates to zero and then the speed command is applied thereafter for forward or reverse accordingly. The extended speed operation using flux weakening control is shown in the Figures 5-30, 5-31 and 5-32. The Motor Phase A current from the current probe, q-axis and d-axis currents are captured in the plots for motor speed at 155RPM, 195RPM and 225RPM. Lastly, the Figure 5-33 and 5-34 show torque/power Vs Speed and torque/current (rms) Vs Speed during the flux weakening operation.

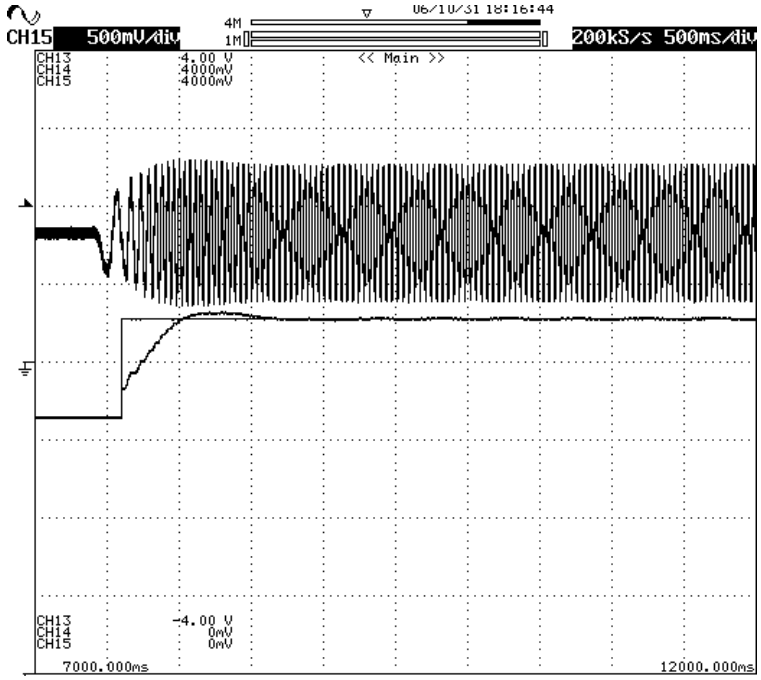

Figure 5-11: (From top to bottom) Phase A current (DSP)-[1V/div], speed command & motor speed-[500mV/div] step change from 0 to 130RPM

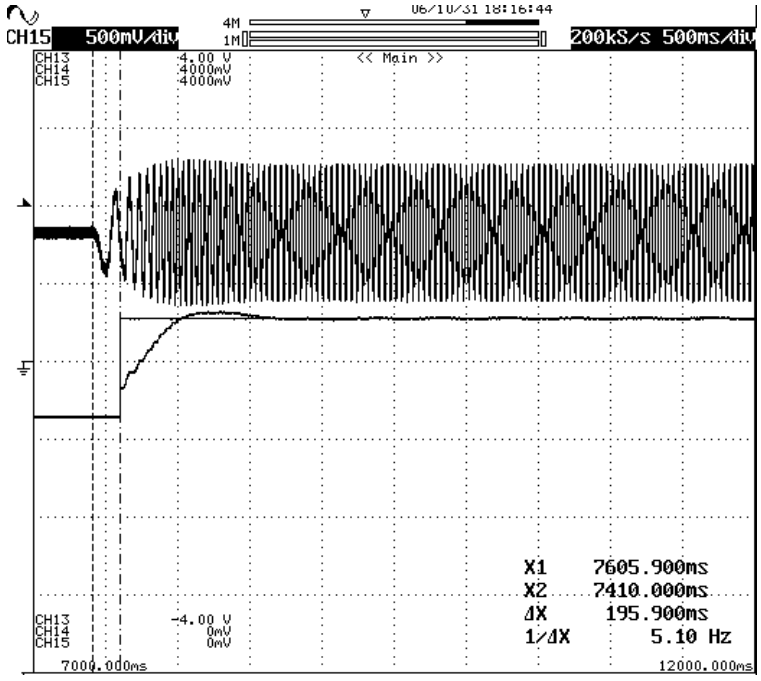

Figure 5-12: (From top to bottom) Phase A current (DSP) –[1V/div], speed command & motor speed-[500mV/div] and cursor difference shows the open-loop start time

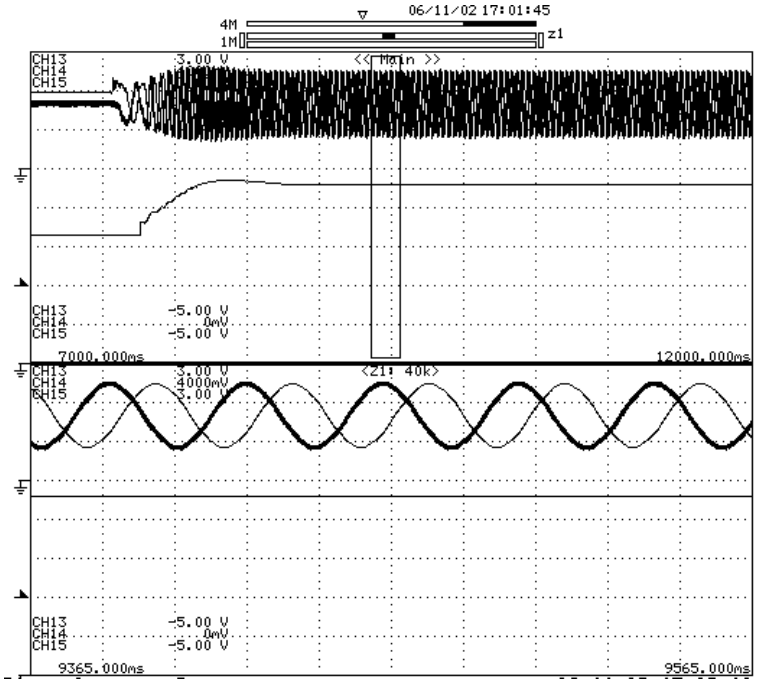

Figure 5-13: (From top to bottom) Phase A current (DSP), phase B current (DSP)-[1V/div] & motor speed-[500mV/div] @130RPM

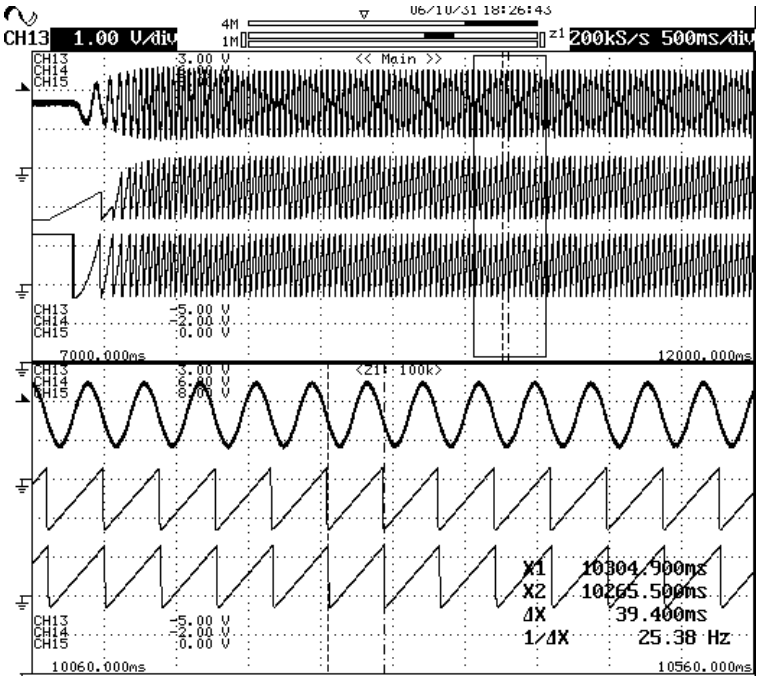

Figure 5-14: (From top to bottom) Phase A current (DSP)-[1V/div], estimated position using one optical sensor and estimated position using sliding observer-[1V/div]

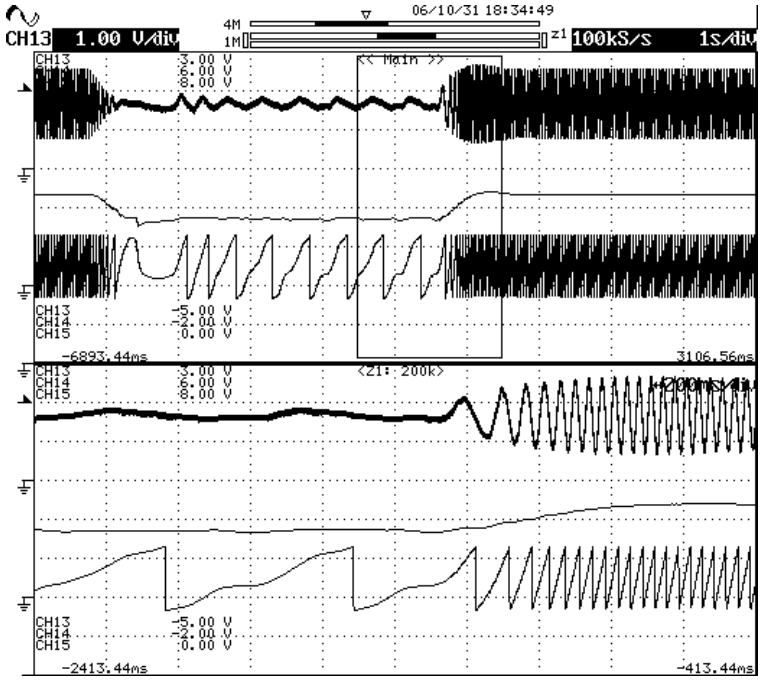

Figure 5-15: (From top to bottom) Phase A current (DSP)-[1V/div], motor speed change-[1V/div] (from 130RPM to 10RPM and back to 130RPM) and estimated position using sliding observer-[1V/div]

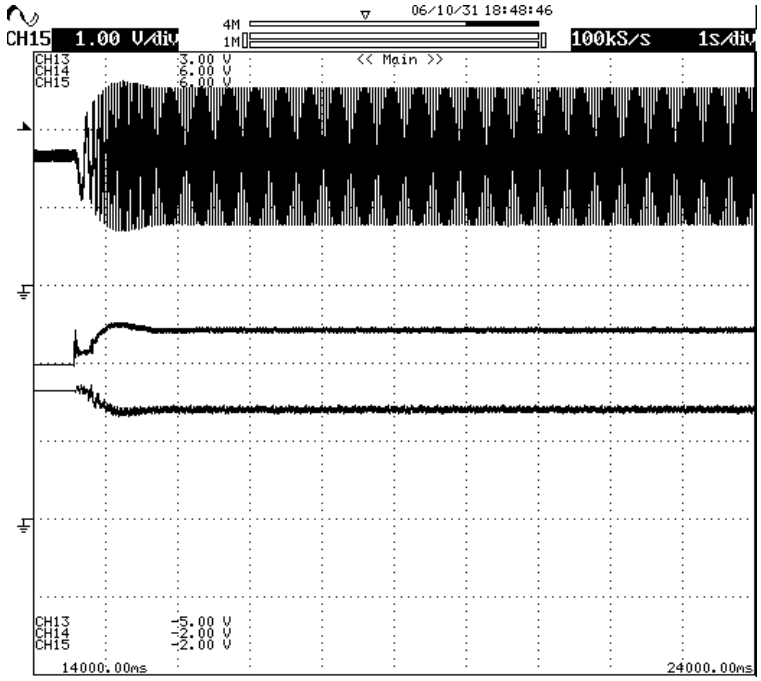

Figure 5-16: (From top to bottom) Phase A current (DSP)-[1V/div], q-axis current and d-axis current in pu-[1V/div]

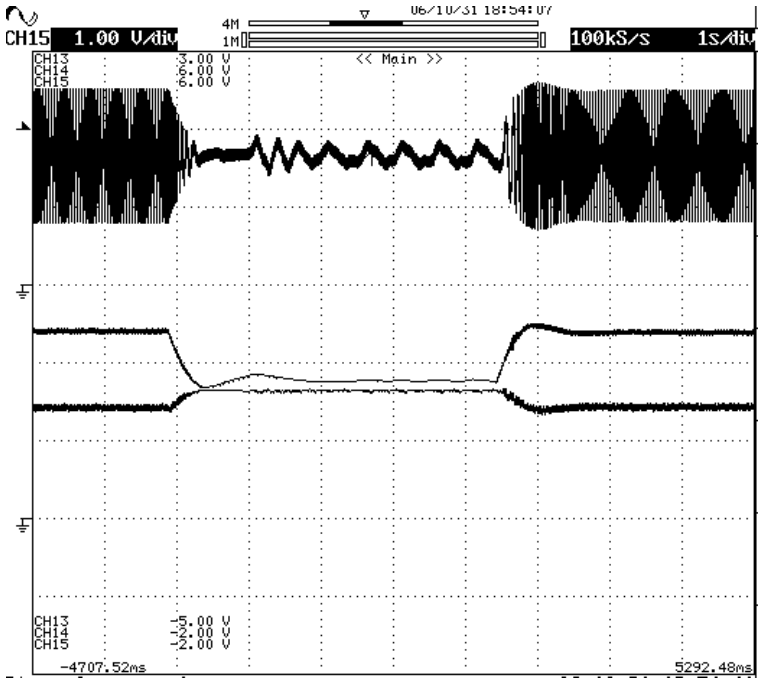

Figure 5-17: (From top to bottom) Phase A current (DSP)-[1V/div], q-axis and d-axis currents-[1V/div] when motor speed is changed from 130RPM to 10RPM and back to 130RPM

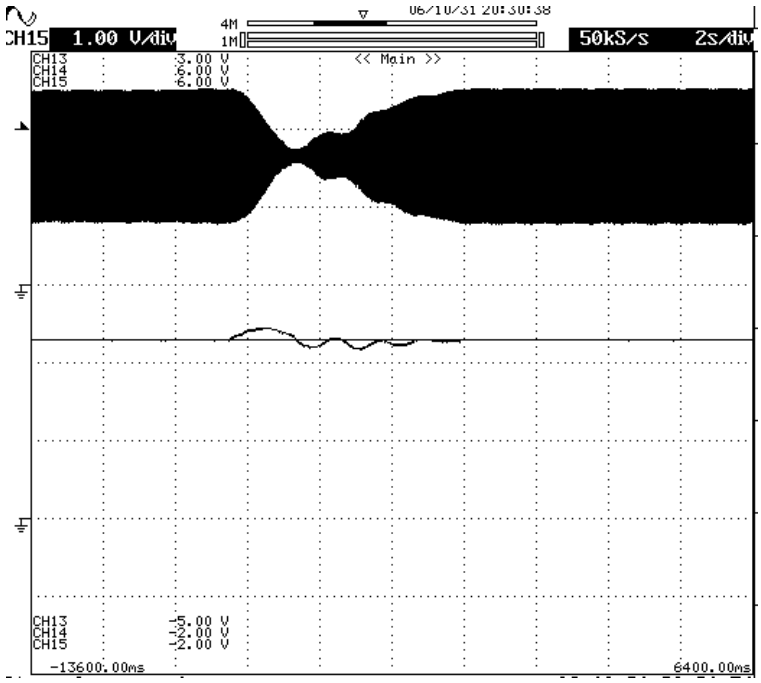

Figure 5-18: (From top to bottom) Phase A current (DSP)-[1V/div], speed command and motor speed-[1V/div] for dynamo load changes

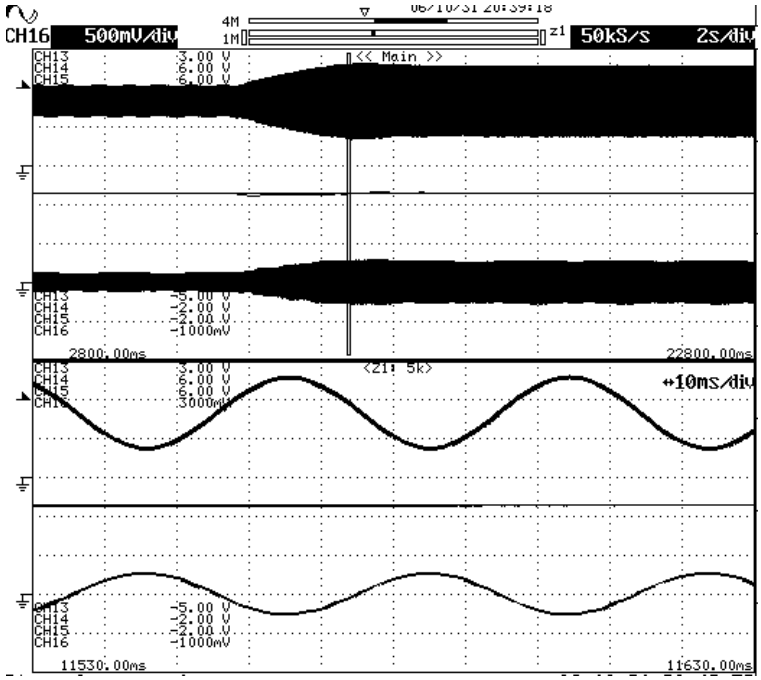

Figure 5-19: (From top to bottom) Phase A current (DSP)-[1V/div], speed command, motor speed-[1V/div] and motor phase A current-[500mV/div with 100mV/A] for dynamo load changes

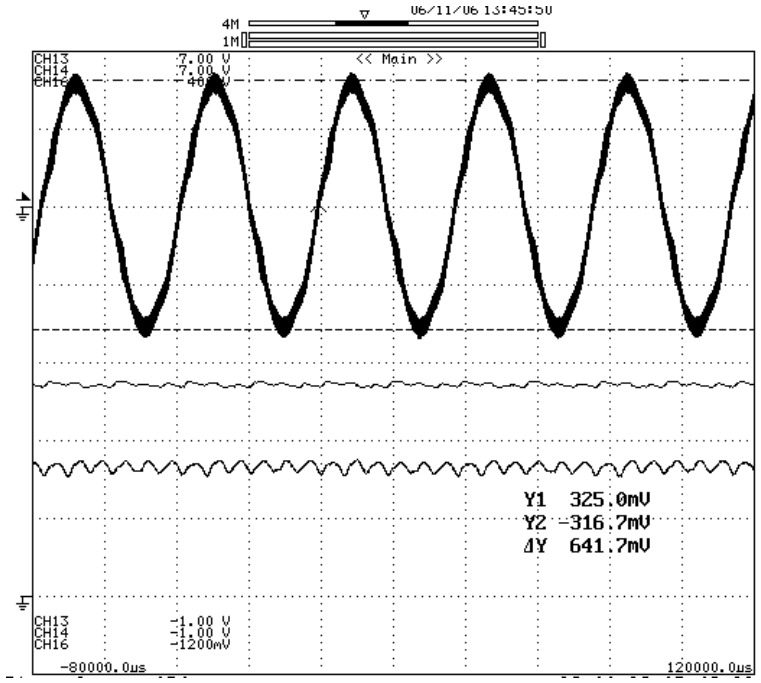

Figure 5-20: (From top to bottom) Motor phase A current-[500mV/div with 100mV/A], q-axis and d-axis current in pu-[1V/div] when d-axis current is zero, (Note: Phase A current is 6.41Apk-pk)

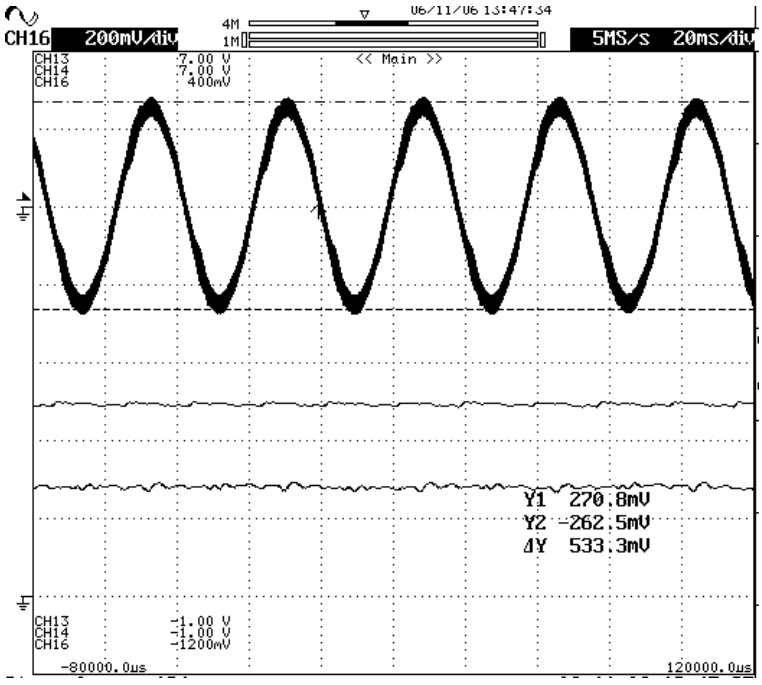

Figure 5-21: (From top to bottom) Motor phase A current-[500mV/div with 100mV/A], q-axis and d-axis current in pu-[1V/div] when d-axis current is based on MTPA, (Note: Phase A current is 5.33Apk-pk)

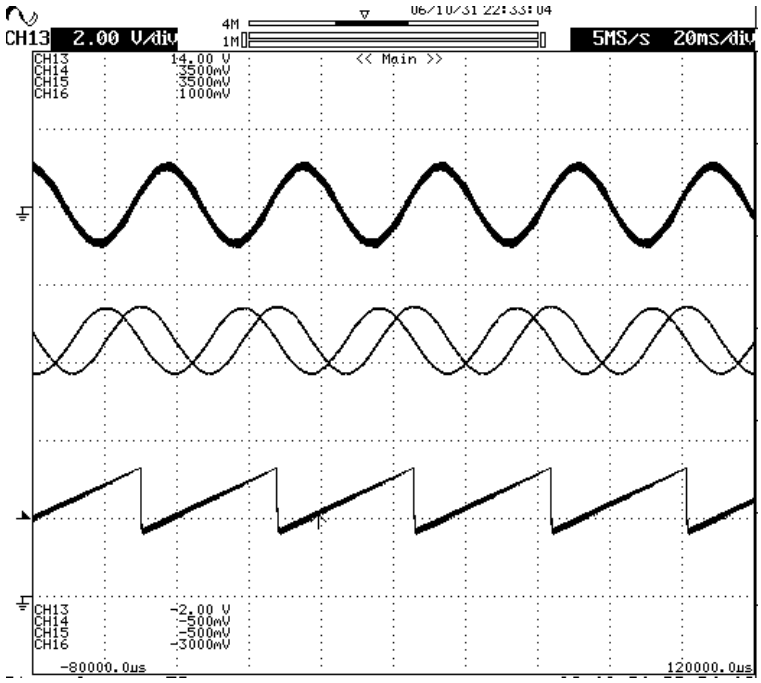

Figure 5-22: (From top to bottom) Motor phase A current-[500mV/div with 100mV/A], stationary frame estimated back-EMFs-[500mV/div] and estimated position-[1V/div] using sliding observer

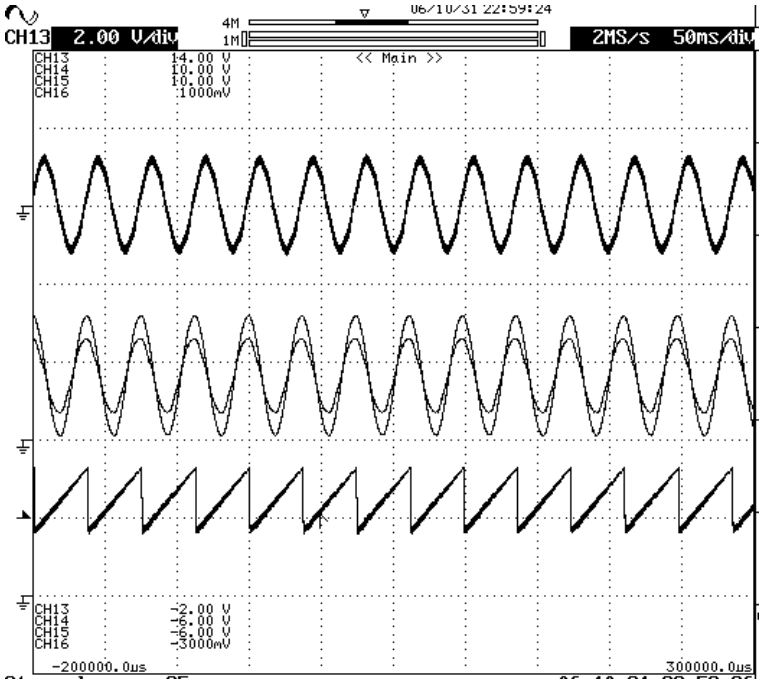

Figure 5-23: (From top to bottom) Motor phase A current-[500mV/div with 100mV/A], stationary frame actual and estimated current in pu-[2V/div] and estimated position-[2V/div] using sliding observer

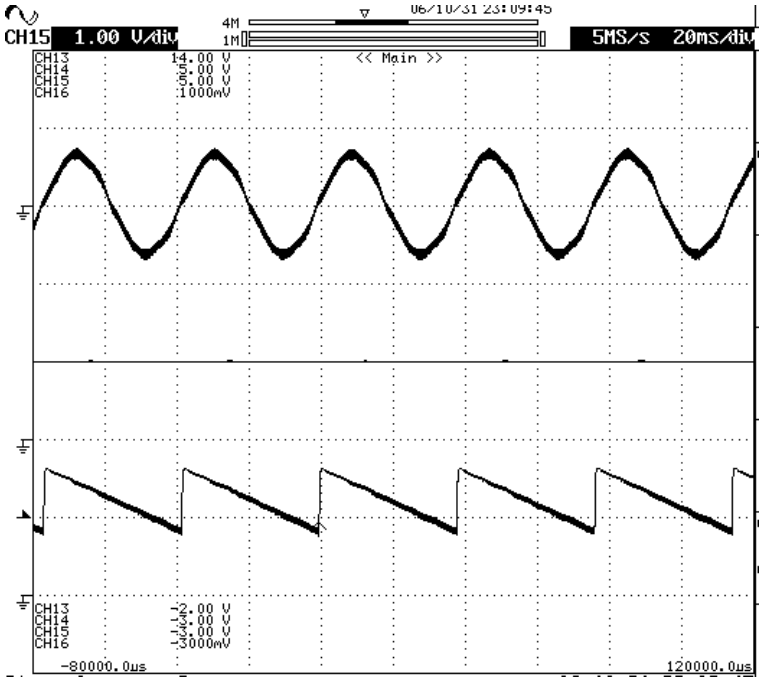

Figure 5-24: (From top to bottom) Motor phase A current, speed command-[500mV/div with 100mV/A], motor speed-[1V/div] (at -130 RPM) and estimated position-[2V/div] using sliding observer when motor running is reversed

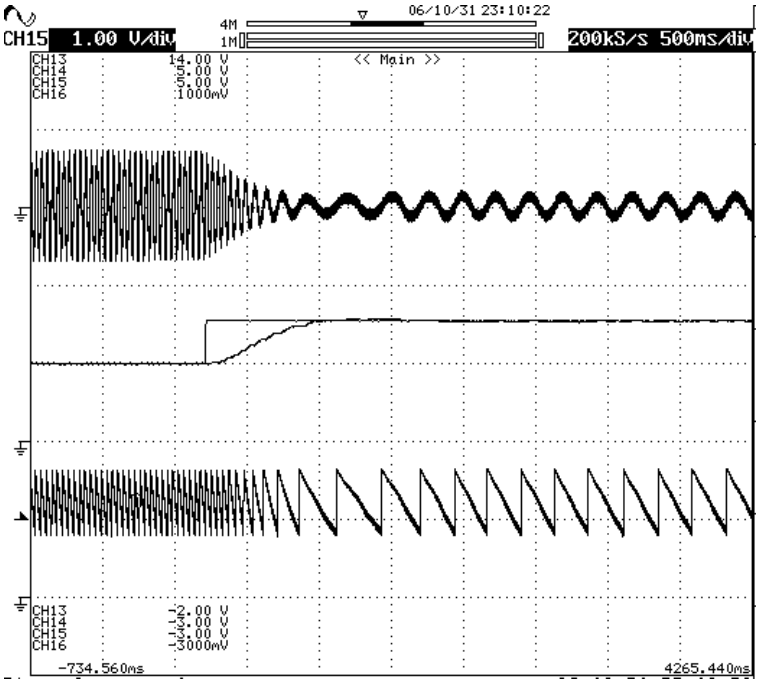

Figure 5-25: (From top to bottom) Motor phase A current-[500mV/div with 100mV/A], speed command, motor speed-[1V/div] and estimated position-[2V/div] using sliding observer when speed is changed from -130 RPM to -10 RPM

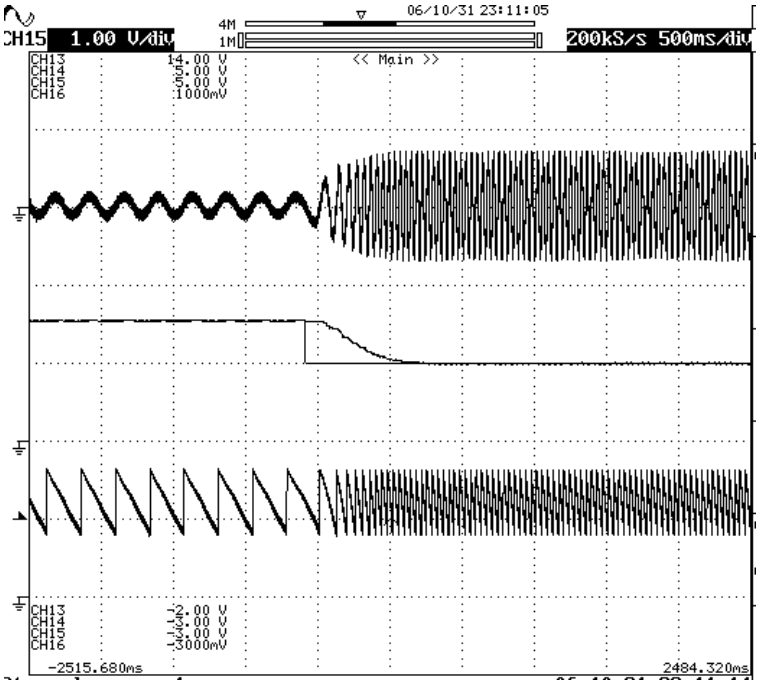

Figure 5-26: (From top to bottom) Motor phase A current-[500mV/div with 100mV/A], speed command, motor speed-[1V/div] and estimated position-[2V/div] using sliding observer when speed is changed from -10RPM to -130RPM

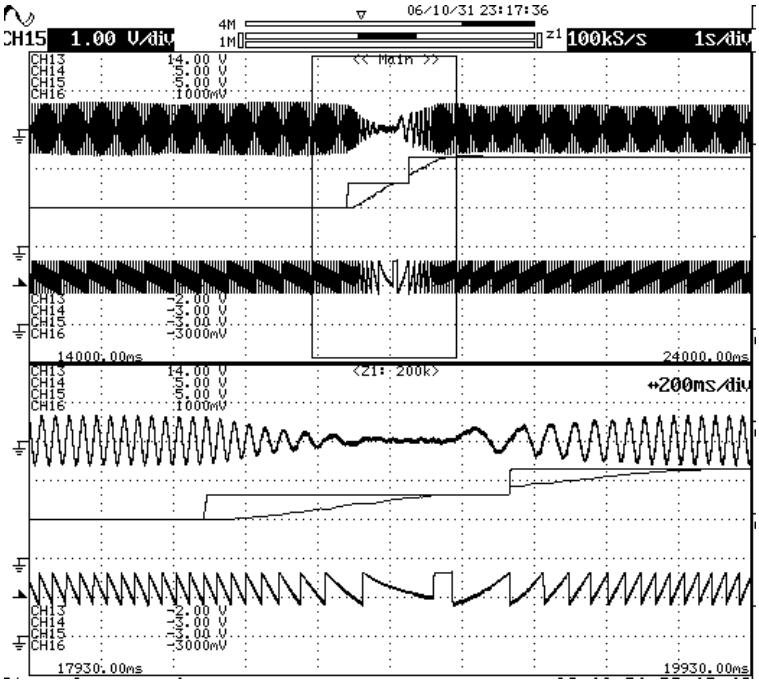

Figure 5-27: (From top to bottom) Motor phase A current-[500mV/div with 100mV/A], speed command, motor speed-[1V/div] and estimated position-[2V/div] using sliding observer when speed is changed from -130RPM to +130RPM with transition zoomed

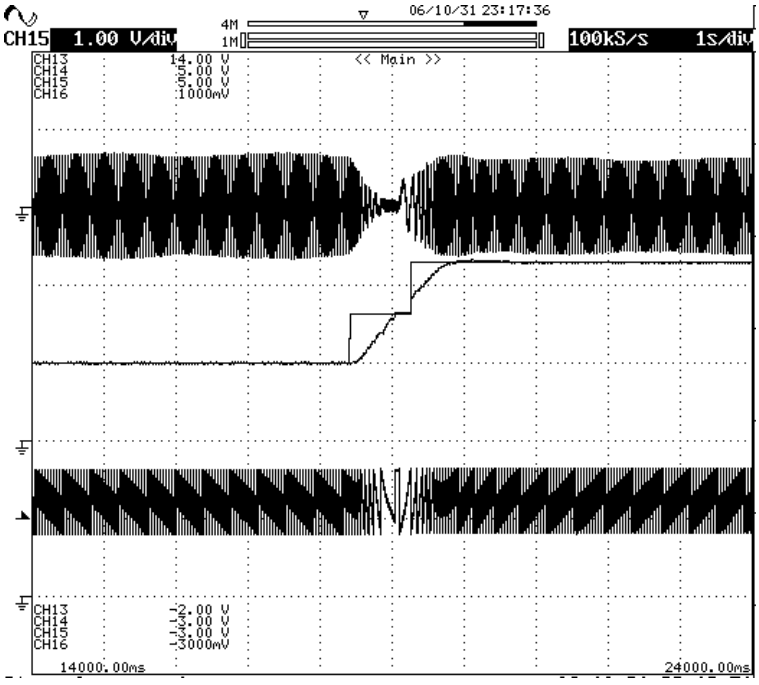

Figure 5-28: (From top to bottom) Motor phase A current-[500mV/div with 100mV/A], speed command, motor speed-[1V/div] and estimated position-[2V/div] using sliding observer when speed is changed from -130RPM to +130RPM

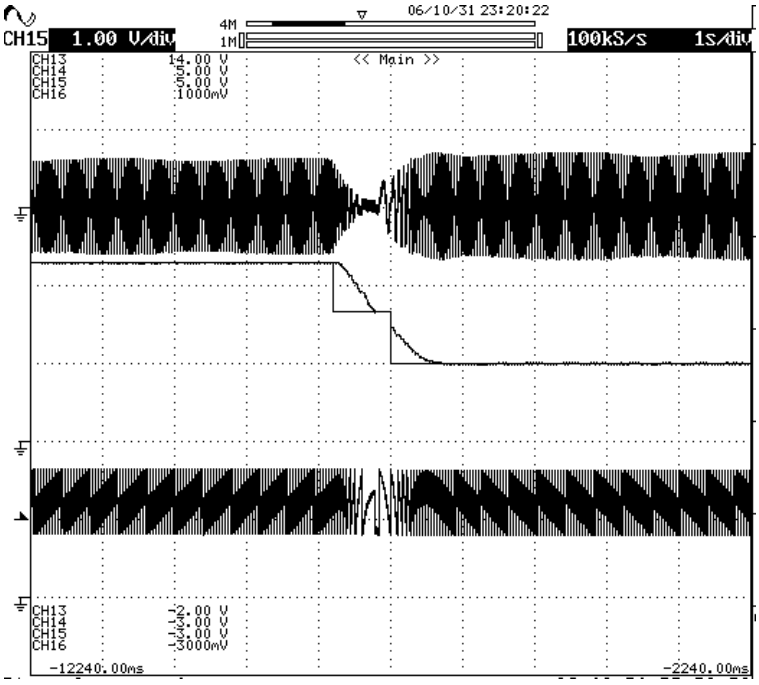

Figure 5-29: (From top to bottom) Motor phase A current-[500mV/div with 100mV/A], speed command, motor speed-[1V/div] and estimated position-[2V/div] using sliding observer when speed is changed from +130RPM to -130RPM

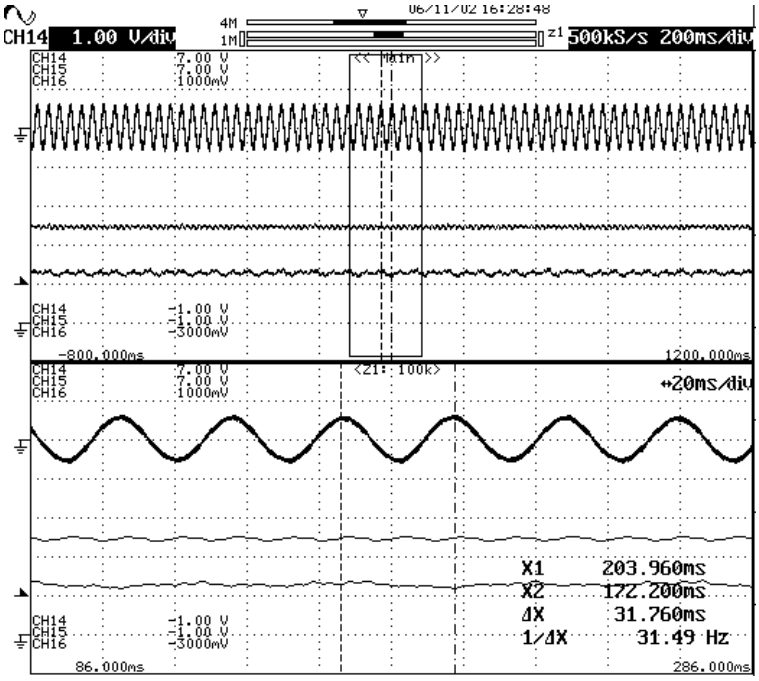

Figure 5-30: (From top to bottom) Motor phase A current-[500mV/div with 100mV/A], q-axis and d-axis currents in pu-[1V/div] for motor speed 155RPM (flux-weakening control)

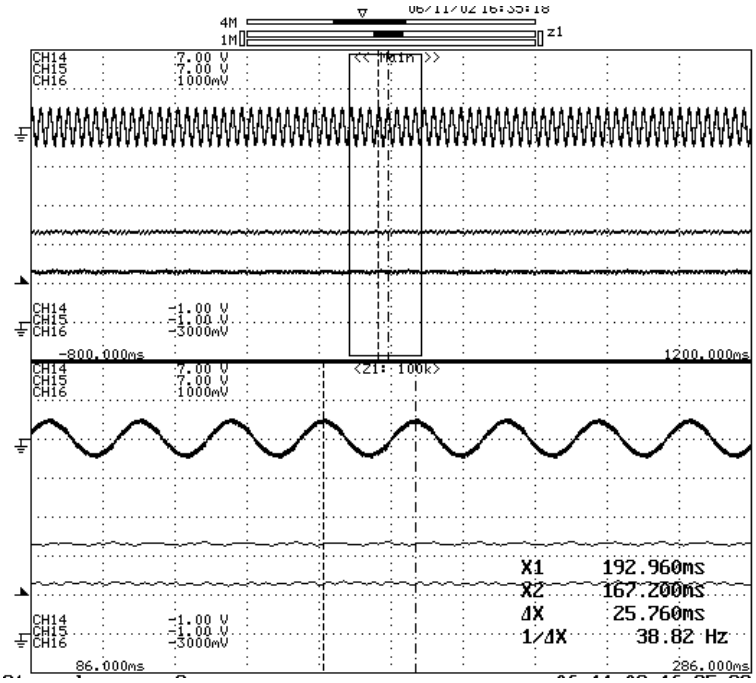

Figure 5-31: (From top to bottom) Motor phase A current-[500mV/div with 100mV/A], q-axis and d-axis currents in pu-[1V/div] for motor speed 195RPM (flux-weakening control)

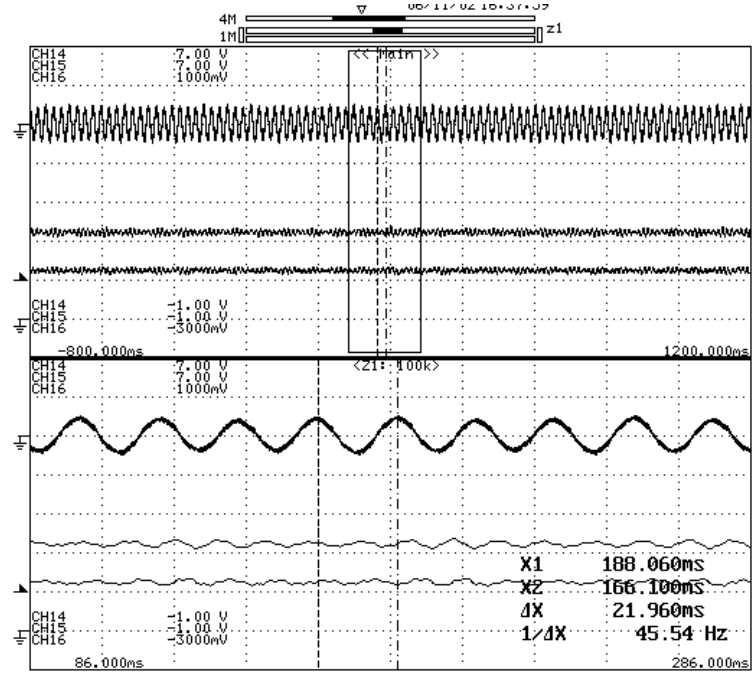

Figure 5-32: (From top to bottom) Motor phase A current[500mV/div with 100mV/A], q-axis and d-axis currents in pu-[1V/div] for motor speed 225RPM (flux-weakening control)

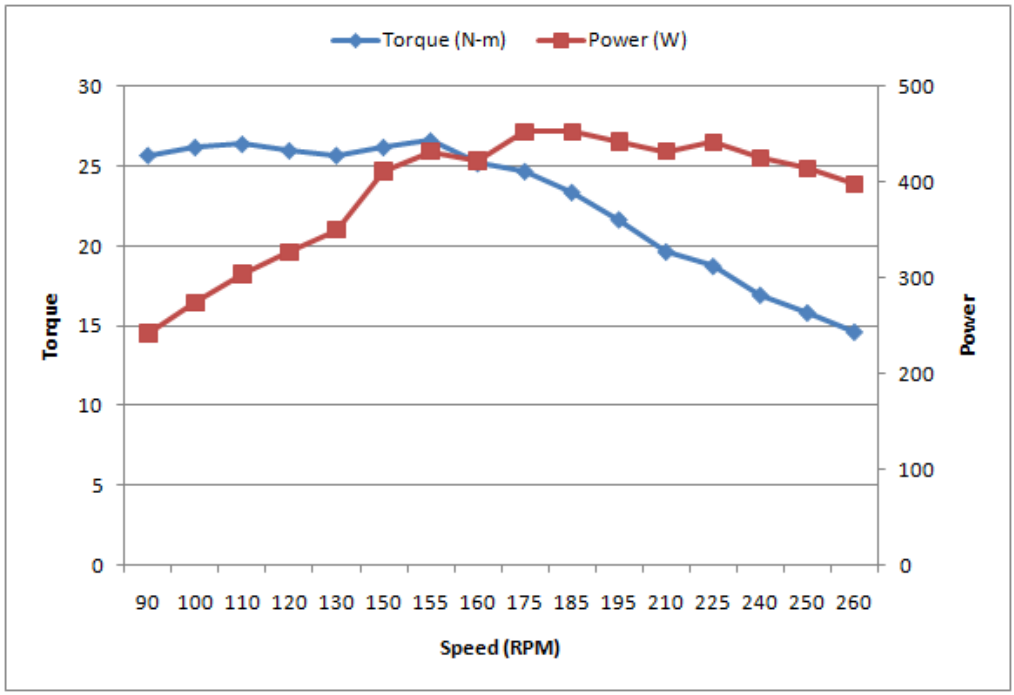

Figure 5-33: Torque, power Vs speed

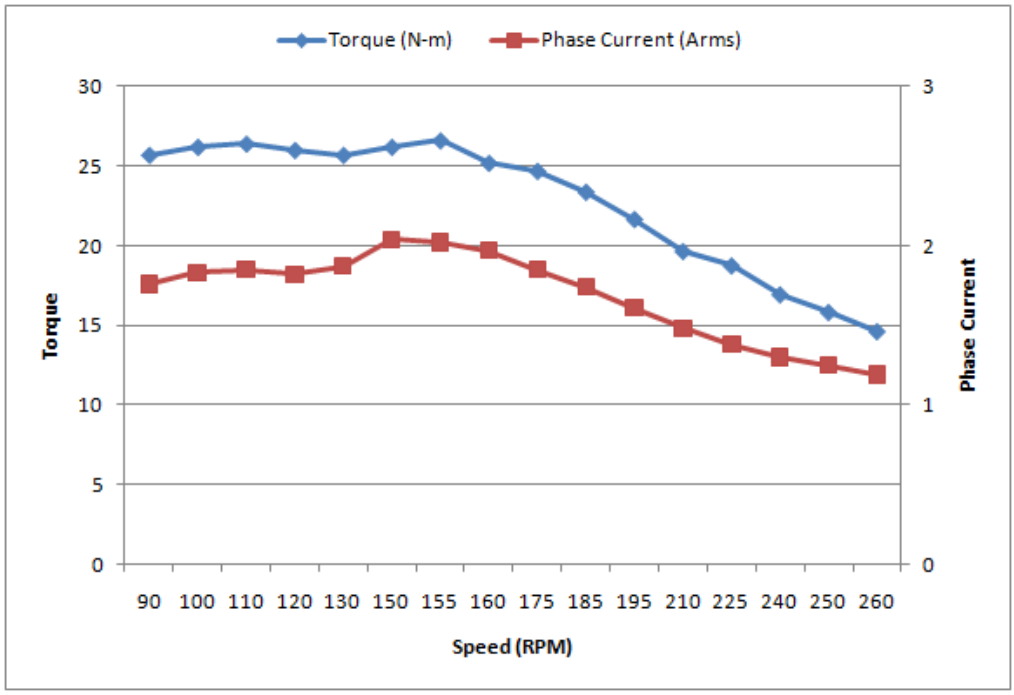

Figure 5-34: Torque, phase current Vs speed

CHAPTER VI

CONCLUSIONS

6.1 Conclusions

This thesis presents the sensorless speed control of PMa-SynRM motor using sliding mode observer. The control schemes are experimented on a prototype PMa-SynRM motor using TMS320F2812 DSP in Advanced Electric machines and Power Electroincs Lab, TAMU. The motor system achieved good dynamic and steady-state performance and is robust to the load and speed variations. The sliding observer sensorless position estimation is robust, works well for speeds as low as 10RPM but fails below this. Also the motor system cannot start from standstill using sliding observer, so open loop start-up was implemented. Further research and feasibility of replacing the open loop start-up with zero speed detection schemes can be carried out.

The motor system was also demonstrated for the forward and reverse running and can also change from forward to reverse and vice verse in real time. The time taken for the operation from forward to reverse or reverse to forward running is almost one sec which can be improved. Next, the flux-weakening capability of the motor system is experimented and the motor was able to run upto 300RPM with almost constant power. Increasing the motor speed beyond this can be investigated, but cannot be guaranteed that it will achieve a very large constant power speed range since the motor is of high

pole number. Lastly, the experimental results presented validate the operation and theoretical analysis.

REFERENCES

[1] P. Vas, *Sensorless and Direct Torque Control*, 1st ed., Oxford: University Press, 1998.

[2] B. K. Bose, "Power electronics and motion control—Technology status and recent trends," *IEEE Trans. Ind. Applicat.*, vol. 29, pp. 902–909, Sept./Oct. 1993.

[3] B. K. Bose, "Variable frequency drives-technology and applications," in *Proc. ISIE 93(Budapest)*, June 1993, pp 1-18.

[4] V. Utkin, J. Guldner and J. Shi, *Sliding Mode Control in Electromechanical Systems*, 1st ed., Philadelphia: Taylor & Francis, 1999.

[5] T. A. Lipo, "Recent progress in the development of solid state ac motor drives," *IEEE Trans. Power Electron.*, vol. 3, pp. 105-117, April 1988.

[6] W. Leonhard, "Adjustable speed ac drives," *Proceedings of IEEE*, vol. 76, pp. 455-471, April 1988.

[7] F. Parasiliti and P. Bertoldi, *Energy Efficiency in Motor Driven Systems*, Berlin: Springer-Verlag, 2003.

[8] R. Gabriel, W. Leonhard, and C. Nordby, "Field oriented control of standard AC motor using microprocessor," *IEEE Trans. Ind. Applicat.*, vol. IA-16, pp. 186–192, 1980.

[9] L. Harnefors, "Design and analysis of general rotor-flux oriented vector control systems," *IEEE Trans. Ind. Electron.*, vol. 48, pp. 383–389, Apr. 2001.

[10] M. Schroedl, "Sensorless control of AC machines at low speed and standstill based on the "INFORM" method," in *Conf. Rec. IEEE-IAS Annu. Meeting*, vol. 1, 1996, pp. 270–277.

[11] P. L. Jansen and R. D. Lorentz, "Transducerless position and velocity estimation in induction and salient AC machines," *IEEE Trans. Ind. Applicat.*, vol. 31, pp. 240–247, Mar/Apr 1995.

[12] P. L. Jansen, R. D. Lorenz, and D. W. Novotny, "Observer-based direct field orientation: Analysis and comparison of alternative methods," *IEEE Trans. Ind. Applicat.*, vol. 30, pp. 945–953, July/Aug. 1994.

[13] N. Bianchi, S. Bolognani, "High-performance PM synchronous motor drive for an electrical scooter", *IEEE Trans. Ind. Applicat.*, vol. 37, no. 5, pp. 1348-1355 September/October 2001.

[14] B. Sneyers, D. W. Novotny and T. A. Lipo, "Field weakening in buried permanent magnet ac motor drives," *IEEE Trans. Ind. Applicat.*, vol. IA-21, pp. 398-407, Mar./Apr. 1991.

[15] T. M. Jahns and V. Blasko, "Recent advances in power electronics technology for industrial and traction machine drives," *Proc. IEEE*, vol. 89, pp. 963–975, June 2001.

[16] T. M. Jahns "Flux-weakening regime operation of an interior permanent-magnet synchronous motor drives," *IEEE Trans. Ind. Applicat.*, vol. IA-23, pp. 681-689, July/Aug. 1987.

[17] D. A. Staton, T. J. E. Miller and S. E. Wood, "Maximizing the saliency ratio of the synchronous reluctance motor," *IEEE Proceedings-B*, vol. 140, no. 4, pp. 249-259, 1993.

[18] T. Matsuo and T. A. Lipo, "Rotor design optimization of synchronous reluctance machine," *IEEE Transactions on Energy Conversions*, vol. 9, no. 2, pp. 359-365, 1994.

[19] T. A. Lipo, A. Vagatti, L. Malesani, and T. Fukao, "Synchronous reluctance motors and drives-a new alternative," *IEEE-IAS Annual Meeting Tutorial*, October 1992.

[20] W. Leonhard, *Control of Electrical Drives*, Berlin: Springer-Verlag, 1985.

[21] K. Uezato, T. Senjyu, and Y. Tomori, "Modeling and vector control of synchronous reluctance motors including stator iron loss," *IEEE Transactions on Industry Applications*, vol. 30, no. 4, pp. 825-834, 1967.

[22] P. J. Lawreson and S. R. Bowes, "Stability of reluctance machines," *IEEE Proceedings*, vol. 118, no. 2, pp. 356-369, 1971.

[23] I. Boldea, L. Tutelea, C. I. Pitic, "PM-assisted reluctance synchronous motor/generator (PM-RSM) for mild hybrid vehicle: electromagnetic design," *IEEE Transaction on Industry Application*, vol. 40, no. 2, pp. 492-498, March/April 2004.

[24] R. Lagerquist, R. B. Betz and T. J. E. Miller, "Dsp96002 based high performance digital vector controller for synchronous reluctance motors," *ICEM Proceeding*, Manchester, Sept 1992.

[25] R.Wu, and G. R. Slemon, "A permanent magnet motor drive without a shaft sensor," *IEEE Trans. Ind. Applicat.*, vol. 27, pp. 1005-1011, September/October, 1991.

[26] M. Naidu and B. K. Bose, "Rotor position estimation scheme of a permanent magnet synchronous machine for high performance variable speed drive," in *Conf. Rec. IEEE-IAS Annu. Meeting*, vol. 1, pp. 48-53, 1992.

[27] H. Watanabe, H. Katsushima, and T. Fujii, "An improved measuring system of rotor position angles of the sensorless direct drive servo motor," in *Proc. IEEE IECON'91*, vol. 1, pp. 165-170.

[28] J. S. Kim and S. K. Sul, "New approach for high-performance PMSM drives without rotational position sensors," *IEEE Trans. Power Electron.*, vol. 12, pp. 904-911, Sept. 1997.

[29] R. Dhaouadi, N. Mohan, and I. Norum, "Design and implementation of an extended kalman filter for the state estimation of a permanent magnet synchronous motor," *IEEE Trans. Power Electron.*, vol. 63, pp. 491-497., July 1991.

[30] A. Bado, S. Bolognani and M. Zigliotto, "Effective estimation of speed and rotor position of a PM synchronous motor drive by a kalman filtering technique," in *Proc. IEEE PESC'92*, vol. 2, pp. 951-957.

[31] T. Low, T. Lee, and K. Chang, "A nonlinear speed observer for permanent magnet synchronous motor," *IEEE Trans. Ind. Electron.*, vol. 40, pp. 307-315, June 1993.

[32] R. B. Sepe and J. H. Lang, "Real-time observer-based (adaptive) control of a permanent magnet synchronous motor without mechanical sensors," *IEEE Trans. Ind. Applicat.*, vol. 28, pp. 1345-1352, November/December 1992.

[33] J. S. Kim and S. K. Sul, "High performance PMSM drives without rotational position sensors using reduced order observer," in *Conf. Rec. IEEE-IAS Annu. Meeting*, vol. 1, 1995, pp. 75-82.

[34] T. Senjyu, M. Tomita, S. Doki, and S. Okuma, "Sensorless vector control of brushless DC motors using disturbance observer," in *Proc. IEEE PESC'95*, vol. 1, pp. 772-777.

[35] J. Hu, D. Zhu, Y. Li and J. Gao, "Application of sliding observer to sensorless permanent magnet synchronous motor drive system," in *Proc. IEEE PESC'94*, vol. 1, pp. 532-536.

[36] Y. S. Han and Y. S. Kim, "The speed and position sensorless control of PMSM using the sliding mode observer with the estimator of stator resistance," in *Proc. IEEE IECON 99*, vol. 2, pp. 1479-1482.

[37] A. Consoli, G. Scarcella, and A. Testa, "Sensorless control of PM synchronous motors at zero speed," in *Conf. Rec. IEEE-IAS Annu. Meeting '99*, vol. 2, pp. 1033-1040.

[38] J. I. Ha, K. Ide, T. Sawa, and S. K. Sul, "Sensorless position control and initial position estimation of an interior permanent magnet motor," in *Conf. Rec. IEEE-IAS Annu. Meeting 2001*, vol. 4, pp. 2607-2613.

[39] D. W. Chung, J. K. Kang, and S. K. Sul, "Initial rotor position detection of PMSM at standstill without rotational transducer," in *Conf. IEMD'99*, pp. 785-787.

[40] M. Schroedl, "Sensorless control of AC machines at low speed and standatill based on the "INFORM" method," in *Conf. Rec. IEEE-IAS Annu. Meeting 1996*, vol. 1, pp. 270-277.

[41] M. J. Corley and R. D. Lorenz, "Rotor position and velocity estimation for permanent magnet synchronous machine at standstill and high speed," in *Conf. Rec. IEEE-IAS Annu. Meeting 1996*, vol. 1, pp. 36-41.

[42] D. Schroëder, C. Schäffner, and U. Lenz, "Neural-net based observers for sensorless drives," in *Proc. 20th Int. Conf. Industrial Electronics Control and Instrumentation (IECON'94)*, Bologna, Italy, 1994, vol. 3, pp. 1599–1610.

[43] T. L. Hsien, Y. Y. Sun and M. C. Tsai, "H∞ control for sensorless permanent magnet synchronous drive," *IEEE Proc. Electr. Power Appl.*, vol. 144, No. 3, pp. 173-181, May 1997.

[44] Y. Yi, D. M. Vilathgamuwa, and M. A. Rahman, "Implementation of an artificial neural-network-based real-time adaptive controller for an interior permanent magnet motor drive," *IEEE Trans. Ind. Appl.*, vol. 39, no. 1, pp. 96-104, Jan./Feb. 2003.

[45] Paul C. Krause, Oleg Wasynczuk and Scott D. Sudhoff, *Analysis of Electric Machinery*, New York: IEEE Press, Inc., 1986.

APPENDIX A

Motor Parameters

PMa-SynRM	Value (unit)
Stator resistance (R_s)	8.25 (Ω)
d-axis inductance (L_d)	180 (mH)
q-axis inductance (L_q)	155 (mH)
Pole Pairs	12 (pair)
back-EMF constant (λ_m)	0.2232 (Wb)
Stator inductance (L_s) (measured @50Hz)	125 (mH)

Motor Ratings

PMa-SynRM	Value (unit)
Torque	28 (N-m)
Speed	130 (rpm)
Maximum Current	5 (A)

VITA

Anil Kumar Chakali received his Bachelor of Engineering degree in electronics and communications from Karnataka Regional Engineering College (now National Institute of Technology Karnataka), Surathkal, India in June 2001. He then worked as a software engineer at Honeywell Technology Solutions Lab, India for five years. In August 2007, he joined the M.S. program of the Department of Electrical Engineering at Texas A&M University, College Station, Texas, with Dr. Hamid A. Toliyat as his advisor, and he completed his M.S. degree in December 2009. His interests include embedded motor controls and power electronics.

Anil Kumar Chakali may be reached c/o Dr. Hamid A. Toliyat, Electric Machines & Power Electronics Laboratory, Department of Electrical Engineering, TAMU 3128, Texas A&M University, College Station, Texas 77843-31287.